Chapter 6: Studies on anti-inflammatory role of compounds derived from rice beer in *in silico*, *in vitro* and *in vivo* models

Chapter 6: Studies on anti-inflammatory role of compounds derived from rice beer in *in silico*, *in vitro* and *in vivo* models

6.1 Introduction

Rice beer prepared in Assam, India has revealed the presence of considerably large amount of salicylic acid in the starter plants (**Chapter 3**) and phenylethyl alcohol in the final produce (**Chapter 2**).

Salicylic acid is a phenolic compound occurring in fruits, vegetables and spices where it aids in protection against pathogenic agents. Salicylic acid has antiinflammatory effects and is an inhibitor of oxidative stress. Most of its pharmacological properties are contributed to the inhibition of prostaglandin synthesis. Suppression of transcription of genes for cyclooxygenase and inhibition of nuclear factor kappa B by salicylic acid are suggested to be the key anti-inflammatory mechanisms of action for salicylates [1]. The anti-inflammatory action of the popular drug aspirin is due to salicylic acid, and its intake may reduce the risk of colorectal cancer [2]. Derivatives of salicylic acid are widely used for treating various ailments. Acetylsalicylic acid is one of the most widely used drug in the world, 4-aminosalicylic acid have been used as an anti-tuberculosis drug, 5-aminosalicylic acid for the treatment of inflammatory bowel diseases and has anti-inflammatory, analgesic, neuroprotective and antitumor and diflunisal as a pain killer and antipyretic agent [3]. A molecule chemically related to salicylic acid, methyl salicylate 2-O-β-D-lactoside that is isolated from *Gaultheria yunnanensis* have been found to have therapeutic potential for treating inflammatory diseases by regulating the NF-κB pathway and pro-inflammatory cytokine production [4]. Also, esters of acetylsalicylic and salicylic acids and their derivatives were found to have much lower gastric ulcerogenic activity then their corresponding acids, when assayed in stress-sensitized rat [5].

2-Phenylethanol (PEA) is an aromatic alcohol encountered in fermented foods and various yeast strains produce PEA from l-phenylalanine via the Ehrlich pathway involving three enzymes [6]. It is an aromatic primary alcohol with rose like odour and occurs naturally in more than 200 foods [7], such as beer, wine, whiskey, olive oil, grapes, green and black tea, apple juice and coffee [8]. It is currently used as a flavouring substance in food products and is considered to be “generally recognized as safe” (GRAS) [9]. It is mostly present in rose oil and also found in some other essential oils like oils of ylang-ylang, neroli, geranium and carnation, and used in a wide variety of consumer products like colognes, *eaux de toilette*,

cosmetics, soaps and detergents [10]. *S. cerevisiae* can produce as the main catabolic phenethyl alcohol when the sole source of nitrogen is tryptophan, phenylalanine or tyrosine [11]. Mutants of yeast resistant to *o* or *p*-fluoro-DL-phenylalanine which were isolated from a *sake* making yeast *S. cerevisae* Kyokai No. 9 have been found to produce large amounts of β-phenylethyl alcohol and its acetate ester, which have rose like flavour [12]. Robust and stress tolerant *S. cerevisiae* strain for production of 2-phenylethanol (PEA) from l-phenylalanine have also been reported [6] which will help in production of PEA on an industrial scale. PEA has been reported to have antimicrobial activity. The metabolic functions in *E. coli* most sensitive to the inhibitory action of PEA have been reported to be the process of enzyme induction and possibly, the synthesis of mRNA [13]. It has also been proposed that the primary effect of PEA is a limited breakdown of the cell cytoplasmic membrane, followed by the inhibition of DNA synthesis and other cellular functions [14,15].

Inflammation in the body is mediated by the arachidonic acids. Three pathways viz. cycloxygenase (COX) enzymes which catalyse the formation of thromboxanes and prostaglandins; the lipoxygenase (LOX) pathway which leads to lipoxins and leukotrienes; and the epoxyeicosatrienoic acids which are products of the cytochrome P450 enzymes are involved in the synthesis of arachidonic acids. Nonsteroidal anti-inflammatory drugs (NSAIDs) are mostly non-selective COX inhibitors which modulate the arachidonic acid cascade. They however cause undesired gastrointestinal and cardiovascular effects, as a result of imbalance in homeostatic eicosanoid production [16]. It has been observed that esterification of the carboxylic acid function of NSAIDs results in compounds having comparable or higher anti-inflammatory activities reduced ulcerogenic effect than the reference compounds [17]. There have been reports of synthesis of NSAIDs by esterification of the carboxylic acids indole-3-acetic acid and lipoic acid with cinnamyl alcohol. These compounds were found to reduce acute inflammation more than the parent acids and were potent inhibitors of soybean lipoxygenase [16]. NSAIDs are carboxylic acids and temporary masking of the acid function reduces the gastrointestinal toxicity due to the direct mucosa contact mechanism. Esterification of acetylsalicylic acid, salicylic acid, flufenamic acid, tolmetin and various other NSAI acids to produce methyl esters have been carried out and these have lower gastric ulcerogenic activity [18]. There are also the naturally occurring esters like caffeic acid phenethylester (CAPE), a phenolic active component of honey bee propolis. This possesses a variety of pharmacological activities like anti- inflammatory, antioxidant, immunomodulatory and anti-cancer effects. It causes inhibition of arachidonic acid release from the cell membrane; thereby inhibiting the

COX-1 and COX-2 activity and also suppresses the activation of gene responsible for COX-2 expression [19].

Considering these aspects, in the present study, an attempt has been made to catalyze esterfication salicylic acid with phenylethyl alcohol using zinc trifluoromethanesulfonate, and subsequently study the anti-inflammatory activity of the newly synthesized salicylic acid phenylethyl ester (SAPE) by targeting the COX-2 enzyme, and also compare its activity with the commercially available NSAIDs ibrupofen and indometacin. Thereafter, SAPE's role as an antioxidative and anti-inflammatory agent was tested in animal models, with an objective of obtaining an easily synthesizable NSAID with less side effects.

6.2 Materials and methods

6.2.1 Materials

The chemicals and reagents used for preparing the test compound were obtained from Sigma Aldrich, USA. The human embryonic human liver cancer cell line (HepG-2) and human epithelial colorectal adenocarcinoma cells line (CaCo-2) were obtained from National Centre for Cell Science (NCCS), Pune, India. CaCo-2 cells were cultured in MEM medium containing 20 % fetal bovine serum, 100 U/mL penicillin, and 100 mg/L streptomycin and HepG-2 cells were cultured in DMEM medium containing 10 % fetal bovine serum, 100 U/mL penicillin, and 100 mg/L streptomycin. The cells were grown in a stable environment with 5 % CO_2 at 37 ºC. The media for animal cell culture were purchased from HiMedia, India and the chemicals were obtained from Sigma Aldrich, USA. The test animals used were white albino rats (*Rattus norvegicus* of Wistar variety) and they were obtained from Defense Research Laboratory (CPCSEA Reg. Number: 1127/bc/07/CPCSEA), Tezpur, Assam. The study was conducted after obtaining institutional animal ethical committee (IAEC) clearance. The rats were housed in controlled environment (20±1) °C, (60±5) % relative humidity and light/dark (12 h:12 h) cycle in polycarbonate micro-isolator cages within individually ventilated racks under specific pathogen-free barrier conditions. The access to rodent diet and water was given *ad libitum*.

6.2.2 Synthesis of novel ester and structural validation

6.2.2.1 $Zn(OTf)_2$-catalyzed selective esterification of salicylic acid and phenylethyl alcohol

To a stirring solution of I_2 (2.0 equiv) and triphenylphosphine (2.0 equiv) in dry acetonitrile (10 mL) salicylic acid (1.0 equiv) was added under a N_2 atmosphere, following which the reaction mixture was stirred for 10 min, and then (5 mol %) of $Zn(OTf)_2$ was added. Stirring was continued for 30 min at 60 °C, and then phenylethyl alcohol (1.1 equiv) in dry acetonitrile was added. The completion of the reaction was monitored by TLC, following which the mixture was cooled to room temperature and the solvent was removed under reduced pressure. The residue was dissolved in ethylacetate and washed with saturated $NaHCO_3$ followed by brine solution. The organic layer was dried over anhydrous Na_2SO_4 and concentrated under reduced pressure. Column chromatography with silica gel and a gradient solvent system of ethylacetate to hexane yielded the target compound [20].

6.2.2.2 NMR and FTIR study for structural validation of the synthesised compound

The C13 and 1H NMR study was conducted in an instrument (ECS-400, JEOL, Japan) and the software used for data acquisition was Delta, Ver. 4.3.6. The test compounds were dissolved in NMR grade chloroform (Merck, India) and the field strength was set at 9.389766[T] (400 MHz).

The FTIR readings were taken in a FTIR spectrophotometer (Spectrum 100, Perkin Elmer, USA). The data were collected in absorbance (A) mode and the wavelength range selected was 4000 cm^{-1} to 400 cm^{-1}. A resolution of 4 cm^{-1} was used while the number of scans per sample was 4.

6.2.3 *In silico* studies with newly synthesized ester and related compounds

6.2.3.1 Chemical structure generation

For molecular docking simulation, the structure salicylic acid phenylethyl ester (SAPE), indometacin and ibrupofen were generated using ChemOffice 2010 (Cambridge Soft, Massachusetts, USA). Molecular docking requires 3D structure of both protein and ligand (these are usually derived from X-Ray/NMR experiments or homology modelling). The 3D

format of the compounds were generated for docking simulations. MM2 force field methods were used for optimizing their geometries [21] and saved as sybyl mol2 file format.

6.2.3.2 Absorption, distribution, metabolism, excretion and toxicity (ADME-Tox) studies

Absorption, distribution, metabolism, excretion and toxicity (ADME-Tox) properties are directly related to the biological effect of drugs and their fate in an organism. Since they are the main cause of failures for candidate molecules in drug design, they should be considered before developing a new drug. *In silico* methods can predict ADME-Tox properties of a compound at an early stage in drug design [22,23]. The *in silico* ADME-Tox tests related to SAPE was carried out using the software ACD/Labs I-Lab 2.0, which is a webbased service that provides instant access to spectral and chemical databases, and predicts properties, including physicochemical, ADME, and toxicity characteristics [24].

6.2.3.3 Molecular docking against COX-2 (PDB ID: 4PH9) enzyme

Docking programs helps in predicting the possible orientation (poses) of ligand in the receptor binding site. The poses are ranked based on a scoring function which is defined by the inter-molecular binding affinity of the complex. Molecular docking of SAPE, indometacin and ibrupofen was carried out against COX-2 enzyme by using Molegro Virtual Docker 6.01 (MVD) in order to understand the molecular interaction that might be responsible for the inhibition of COX-2 activity computationally. The steps involved in molecular docking of the compounds against COX-2 enzyme involved cavity prediction and docking computation [25].

6.2.3.3.1 Cavity prediction

The cavity detection program of MVD was used to predict the potential ligand binding site of the COX-2 enzyme. The methodology adopted to find out the potential binding sites was a grid based cavity prediction algorithm. A discrete grid (resolution of 0.8 Å) covering the protein was created, then a sphere (1.4 Å radius) was placed and Van der Waals radii of the protein atoms was used to determine whether the sphere overlaps with other spheres. Then each accessible grid point was checked for being part of a cavity from the current grid point in a randomly chosen direction. The chosen direction was followed until the grid boundaries are

hit, thereby checking if any inaccessible grid point is hit on the way. This was repeated several times, and points were marked as being part of a cavity if the percentage of lines hitting an inaccessible volume were larger than a given threshold which could be tuned according to the enclosed cavities. Finally the connected regions were determined by checking if two grid points are neighbours. The regions with a volume below 10.0 $Å^3$ were discarded as irrelevant and the volume of a connected set of grid points was estimated as the number of grid point times (x) the volume of a unit grid cell. Ranking of the cavities found was done according to their volume [26].

6.2.3.3.2 Docking computation

For docking simulations, a tolerance of 1.7 and strength of 0.7 were set for bond flexibility of the compounds and the side chain flexibility of the amino acids surrounding the vicinity of the cavity. For the multiple cluster poses, the root mean squared deviation (RMSD) threshold were set at 2.00 Å. In order to ensure conformations to the lowest energy state, maximum iteration of 1,500, simplex evolution size of 50 and minimum of 100 runs for each compound was set in the docking algorithm. There were five poses of each molecule in the protein complex and the resulting poses were visualized in the Pose Organiser. From the top docking hits, the best pose of each compound were selected for the ligand-protein interaction analysis.

6.2.3.4 Molecular dynamics (MD) simulation study of the SAPE-COX-2 docked complex

MD simulation studies were carried for the top docking hits against the COX-2 protein (protein-ligand docked complex) and the system was processed using Gromos 43a1 force field. The PRODRG server was used to generate the ligand topology and atom charges. The charge values were set to full, the chirality was set to default and there was no further energy minimization [26]. The protein-ligand system was immersed in a cubic water box with the energies of the systems being minimized for at least 1000 steps of steepest descent. Further, equilibration of the systems were done for 100 ps at constant temperature and pressure, with NVT (canonical) and NPT (isothermal–isobaric) equilibration. The equilibrated structures generated were subjected to 20 ns MD simulation production, following which the trajectory was analysed and plotted for RMSD backbone of the COX-2 protein and the COX-2-ligand docked complex.

6.2.4 Test for *in vitro* cytotoxicity of SAPE in animal cell line models

6.2.4.1 Isolation and culture of human primary peripheral blood mononuclear cells (PBMC) and RBCs

Human blood samples were collected voluntarily in the Health Centre of Tezpur University, Tezpur, Assam. Isolation performed according to the method described by Borah et al. [27] by density gradient centrifugation. The isolated human lymphocyte cells (PBMC) ($3x10^3$ in 200 µl) were seeded in RPMI-1640 media supplemented with 10% FBS in 96 well plates. Initially, cells were incubated (at 37 °C in 5 % CO_2) for 8 h in RPMI-1640 without FBS. The cells were then treated as per experimental requirement and maintained with the inclusion of FBS for 24 h. RBCs were isolated and washed three times with PBS (pH 7.4) and then centrifuged at 2000 rpm for 10 min. Then 2 % of the erythrocyte suspension (ES) was re-suspended in saline solution.

6.2.4.2 Membrane stability assay of SAPE

The reaction mixture for this assay contained 100 µL of ES, 0.1 % Triton X-100 and 25, 50 or 100 µg/mL of SAPE in 96-well microplates. This was incubated for 60 min at 37 °C under constant agitation and then centrifuged at 2000 rpm for 10 min. The release of hemoglobin was determined by photometric analysis of the supernatant at 576 nm. Complete hemolysis was achieved using 0.1 % Triton X-100 (positive control) yielding the 100 % hemolysis and PBS (negative control) yielding the 0 % hemolysis [28].

6.2.4.3 Test for cytotoxic effect of SAPE by MTT assay

The *in vitro* cytotoxicity of SAPE was assessed using the standard MTT [3-(4,5-dimethyl-2-thiazolyl)-2,5- diphenyl-2-H-tetrazoliumbromide] assay [29] with PCMB and two other cell lines (CaCo-2 and HepG-2). Cells ($2x10^3$) were seeded in a 96-well plate and treated with increasing concentrations 25, 50, 100 and 200 µg/mL of SAPE for 48 h at 37 °C, 5% CO_2. Then, 20 µl of MTT solution (5 mg/mL in PBS) was added to each well and the plate was incubated for another 4 h at 37 ºC. The medium was removed and 200 µl DMSO was added to each well to dissolve the formazons, and after 10 min of mechanical shaking, the optical density

was measured at 570 nm in micro plate reader. The cell viability inhibitory ratio was calculated in relation to control cells cultured in drug-free media according to Eq. 6.1. All experiments were repeated at least three times.

$$\text{Inhibitory ratio } \% = \left(\frac{\text{Acontrol} - \text{Acontrol}}{\text{Acontrol}} \right) \times 100\% \quad \text{Eq. (6.1)}$$

6.2.4.4 Test for cytotoxic effect of SAPE in CaCo2 cells by Alamar Blue® assay

To determine cell viability, Alamar Blue® was added to cells in a 96-well plate for 2 h at 37 °C, 5 % CO_2. The cytotoxicity of the tested samples was performed by resazurin reduction assay as previously described by O'Brien et al. [30].

6.2.5 In vivo study for anti-inflammatory role of SAPE in animal model

6.2.5.1 Experimental design

A pre-treatment model of drug administration was used in this study i.e. drug was administered before the onset of diseased condition. All the rats were 2 months old when taken for experimentation. They were divided into five groups in a randomized manner with equal number of males and females. Group RG-CI: colitis induced group without any treatment (n=8); Group RG-CF: colitis free control group without any treatment (n=8); Group RG-SP: colitis induced group treated with SAPE (n=8); Group RG-IM: colitis induced group treated with indometacin (n=8) and RG-PO: paw oedema induced model group (n=8). Initial weight of the rats is shown in Table 6.1.

Table 6.1 Initial weight of the rats

Group	Body weight (g)
RG-CI	167.88±15.30
RG-CF	151.88±27.45
RG-SP	156.38±26.93
RG-IM	163.75±22.33
RG-PO	160.38±12.03

Note: Average weight of n=8±standard deviation (male =4; female =4)

6.2.5.2 Pre-test in paw oedema model

This was done using a digital plethysmometer (Orchid Scientific, India) according to Upadhyay et al. [31]. Paw oedema was induced in the RG-PO group of rats by injecting 0.15 mL of 0.1 % carrageenan (Sigma Aldrich, USA) in sterile normal saline solution into the sub-plantar region just below the lateral malleolus of both left paws and SAPE (10 mg/kg body weight) and indometacin (Indicap®, Jagsonpal Pharmaceuticals Ltd., India) dissolved in 5 % tween 80 was administered by a trans-dermal route. The controls received only 5 % tween 80. The paw volume was measured before and after carrageenan injection at 1, 3 and 5 h. Each paw volume was obtained from the average of 3 readings. The paw oedema was expressed according to Eq. 6.2.

$$\%\, Oedema \;=\; \left[\frac{V_t - V_o}{V_o} \times 100\right] \qquad \text{Eq. (6.2)}$$

Where, V_t = volume at time t after treatment, V_0 = volume at time 0.

6.2.5.3 Administration of drug and induction of colitis

Starting from day 1, SAPE and indometacin mixed in a suspension of gum acacia and deionised water were administered to all the members of the respective groups (Group RG-SP and RG-IM) using a feeding needle at dosages of 250 mg and 1.5 mg per kg body weight (Fig 1(i)). This was done in the morning hours in between 9 to 10 am every day. This was continued till the 16th day, when 4 h after the last SAPE dose rats of group RG-CI, RG-SP and RG-IM were challenged with intraperitoneal injection of lipopolysaccharides from *Escherichia*

coli 0111:B4 (L2630-25MG, Sigma-Aldrich, USA) at a dose of 5 mg/kg body weight (Fig 1(ii)). All the rats were euthanized 24 h after LPS challenge by CO_2 asphyxiation. Post mortem, colons and small intestines were dissected and flushed with cold 1x phosphate-buffered saline (PBS) containing penicillin/streptomycin (100 I.U./mL penicillin and 100 µg/mL streptomycin) with a protease inhibitor cocktail (P8340-1ML, Sigma-Aldrich, USA) to remove faecal contents, and then opened lengthwise and washed extensively with PBS. Then segments of 0.5-1.0 cm in length which is 2 cm away from the anus were collected and fixed in 10 % neutral buffered formalin. The samples were stored in pyrogen/endotoxin-free tubes and kept frozen at –80 °C prior to analysis.

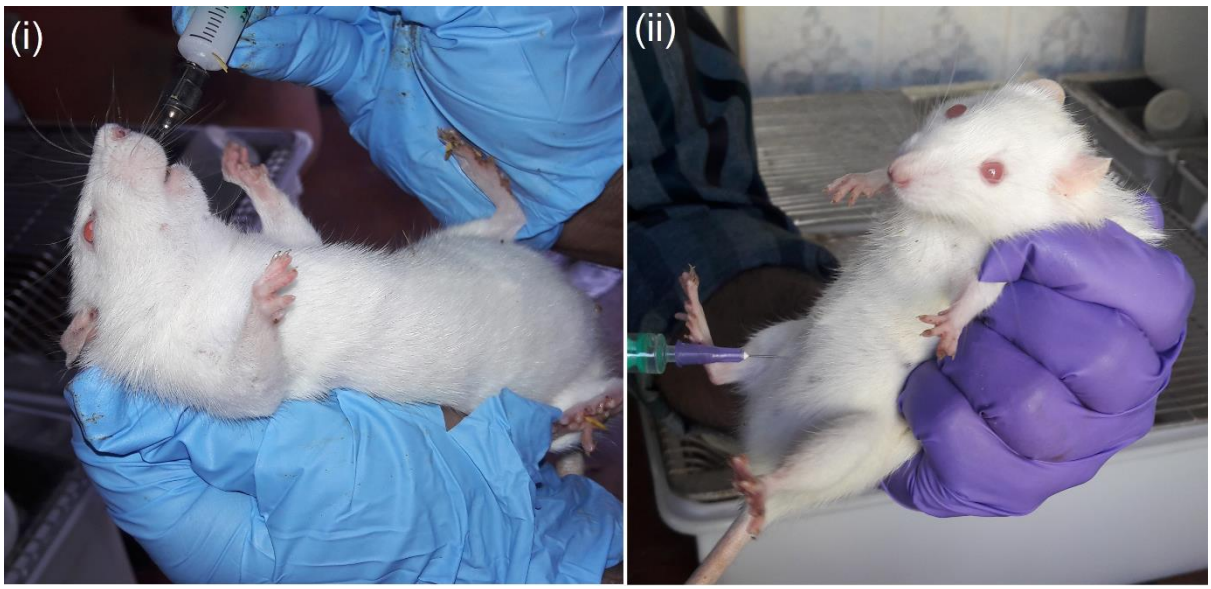

Fig 6.1 (i) Treatment of drugs to the rats using feeding needle (ii) induction of colitis in rats by intraperitoneal injection of lipopolysaccharides

6.2.5.4 Measurement of change in body weight

The body weights of all the rats in all the groups were recorded each day in an electronic balance before the treatment. The rate of body weight gain in each mouse was defined by the Eq. 6.3.

$$Weight\ gain\ (\%) = \frac{Weight\ each\ day - Weight\ at\ day\ 0}{Weight\ at\ day\ 0} \times 100 \qquad \text{Eq. (6.3)}$$

6.2.5.5 Evaluation of disease activity index (DAI)

The DAI was used to evaluate the grade and extent of intestinal inflammation. DAI score were calculated by adding combined scores for weight loss, stool consistency, and faecal bleeding, and dividing this sum by three. The scoring for disease activity index is shown in Table 6.2 [32].

Table 6.2 Disease activity index score table

Score	Body weight loss (%)	Stool consistency	Faecal bleeding
0	0	Normal	Normal
1	1-5		
2	5-10	Loose	Occult bleeding
3	10-15		
4	>15	Diarrhoea	Gross bleeding

Note: Normal stool: shaped stool; Loose stool: pasty unformed stools which do not adhered to the anus; Diarrhoea: watery stools which adhered to the anus

6.2.5.6 Scanning electron microscope (SEM) study of intestinal morphological changes

The tissues were cut into sections of 2-3 mm in size and fixed with 3% glutaraldehyde. Then washed with three changes 0.1M sodium cacodylate buffer, each of 15 min at 4 °C. Again fixed with 0.1% osmium tetroxide in 0.1M sodium cacodylate buffer and washing was repeated. Dehydration was done in series of 30 % to 100 % acetone, each of 15 min and two changes at 4 °C. They were then dried by immersing in tetra methyl silane for 5 min with two changes at 4 °C and then brought to room temperature. The microstructures were investigated using a SEM (JEOL JSM-6390LV, SEM, Oxford). Samples were placed in a brass stub using double-sided tape and coated with a fine layer of gold (about 35 mm thick) using a sputter gold coater. Sample micrographs were observed at a magnification of 500x and 1000x at an accelerating voltage of 20 kV.

6.2.5.7 Antioxidant activity assays

The level of lipid peroxidation in the tissues was analysed using the lipid peroxidation assay kit (MAK085, Sigma-Aldrich, USA). Tissue (10 mg) was homogenized on ice in 300 µL of the malondialdehyde (MDA) lysis buffer containing 3 µL of BHT (100x). It was then centrifuged at 13,000 x g for 10 minutes and 200 µL of the supernatant was added to 600 µL of TBA solution and incubated at 95 °C for 60 min. After cooling to room temperature, the absorbance was measured at 532 nm. A standard curve of MDA ranging from 0 to 20 nmole was also constructed and the concentration of MDA in the sample was calculated according to Eq. 6.4.

$$Concentration\ of\ MDA = (\frac{S_a}{S_v}) \times D \qquad \text{Eq. (6.4)}$$

Where, Sa = amount of MDA in unknown sample (nmole) from standard curve; Sv = sample volume (mL) added and D = sample dilution factor.

The content of catalase (CAT) was determined using a catalase assay kit (A22180, Invitrogen, USA). Tissues (10 mg) were homogenized in 200 mL of reaction buffer, centrifuged at 13,000 x g for 10 min. Then 25 µL of each supernatant was mixed with 25 µL of 40 µM H_2O_2 solution in a 96-well microplate (941196, Tarsons, India) and incubated for 30 min at room temperature. Then 50 µL of Amplex® Red/HRP solution was added to the mixture and further incubated for 30 min at 37 °C in the dark. The absorbance was then measured at 560 nm in a microplate reader (GloMax Explorer, Promega, USA). The catalase concentration was calculated from the standard curve of catalase (0 to 4.0 U/mL) where 1 unit is defined asthe amount of enzyme that will decompose 1.0 µmole of H_2O_2 per minute at pH 7.0 at 25°C.

The assay for γ-glutamyltransferase (GGT) activity was performed using a GGT activity assay kit (MAK089, Sigma-Aldrich, USA). The tissues (10 mg) were homogenized in 200 mL of ice-cold GGT assay buffer, centrifuged at 13,000 x g for 10 minute. Then 10 µL of the supernatant was added to the wells of 96 well plate. And the volume was made to 100 µL with GGT assay buffer. To this, 90 µL of GGT substrate solution was added and the plate was incubated at 37 °C for 3 min ($T_{initial}$) after which the absorbance was taken at 418 nm [$(A_{418})_{initial}$]. pNA standards ranging from 0 to 40 nmole/well were also taken. Incubation was continued at 37 °C taking measurements every 5 minutes until the value of the most active sample became greater than the value of the highest standard. The change in measurement (ΔA_{418}) till final time (T_{final}) was calculated. The amount of pNA generated (B) was calculated by comparing the ΔA_{418} of each sample to the pNA standard curve. The GGT activity was

calculated from the Eq. 6.5 where one unit of GGT is the amount of enzyme that will generate 1.0 µmole of *p*NA per minute at 37 °C.

$$GGT\ Activity = \frac{B \times Sample\ dilution\ factor}{T \times V}\ \text{nmole/min/mL} \qquad \text{Eq. (6.5)}$$

Where,T_{final}, T=reaction time = $T_{final} - T_{initial}$(minutes) and V = sample volume (mL) added to well.

The glutathione S-transferase (GST) activity assay was performed using the GST assay kit (CS0410, Sigma-Aldrich, USA). Tissues (10 mg) were homogenized in 200 mL of sample buffer and 10 µl of the extract was mixed with 1 mL of substrate solution consisting of 980 µl of Dulbecco's phosphate buffered saline, 10 µl of 200 mM L-glutathione reduced and 10 µl of 100 mM 1-chloro-2,4-dinitrobenzene (CNDB) in a quartz cuvette. The absorbance was read every 30 s at 340 nm over a period of 5 minutes after a lag time of 1 minute. The absorbance values were plotted against time and the change in absorbance [(ΔA_{340})/min] was calculated from the linear range of the plot using the Eq. 6.6 and the GST specific activity was calculated from the Eq. 6.7.

$$(\Delta A_{340})/\min = \frac{A_{340}(final\ read) - A_{340}(initial\ read)}{Reaction\ time\ (min)} \qquad \text{Eq. (6.6)}$$

$$\text{GST specific activity} = \frac{(\Delta A_{340})/min \times V(ml) \times dil}{\varepsilon_{mM} \times V_{enz}(ml)}\ \mu\text{mol/mL/min} \qquad \text{Eq. (6.7)}$$

Where, *dil*= the dilution factor of the original sample; ε_{mM} ($mM^{-1}cm^{-1}$) = the extinction coefficient for CDNB conjugate at 340 nm = 9.6 mM^{-1}; *V* = the reaction volume = 1 mL; V_{enz}= the volume of the enzyme sample tested.

6.2.5.8 Pro-inflammatory biomarkers analysis by ELISA

To the tissue samples(100 mg), 8 volumes of RIPA buffer with 1 mM PMSF was added in 100 µL increments and homogenized thoroughly with a probe sonicator (UW2070, Bandelin Electronic, Berlin, Germany). The lysate was incubated on ice for 30 minutes, with occasional vortexing and then centrifuged for 10 min at 13,000×g and 4 °C. The protein content in the supernatant was determined spectrophotmetrically and was further diluted 1:10 to 1:100 with standard diluent buffer prior to analysis.

The assay for interleukin 6 (IL-6) was performed using the mouse IL-6 ELISA kit (KMC0061, Invitrogen, USA). To theIL-6 antibody coated microtiter wells in 96 wells plate,

100 µL the sample extracts, standards (0 - 250 pg/mL Ms IL-6) and controls were added and incubated for 2 h at room temperature. The wells were washed with wash buffer and 100 µLof Ms IL-6 biotin conjugate solution was added into each well except chromogen blanks and incubated for 30 min at room temperature. After washing again, 100 µL of streptavidin-HRP solution was added into each well except the chromogen blanks and incubated for 30 min at room temperature. Again the wells were washed and 100µL of stabilized tetramethylbenzidine (TMB) chromogen was added to each well and incubated for 30 min in the dark. Finally, 100 µL of stop solution was added to each well, mixed gently and the absorbance was read at 450 nm. The unknown concentrations were read from the Ms IL-6 standard curve and multiplied by the dilution factors.

Tumor necrosis factor alpha (TNF-α) was assayed by using the mouse TNF-α ELISA kit (KMC3011, Invitrogen, USA). The sample extracts (100 µL), standards (7.8 - 250 pg/mL Ms TNF-α) and controls were added to the TNF-α antibody coated microtiter wells in 96 wells plate, and then 50 µL of Ms TNF-α biotin conjugate solution was added into each well except chromogen blanks and incubated for 90 min at room temperature. Thereafter wells were washed with wash buffer and 100 µL of 1X streptavidin-HRP solution was added into each well except the chromogen blanks and incubated for 30 min at room temperature. The wells were again washed and 100 µL of stabilized tetramethylbenzidine (TMB) chromogen was added and incubated for 30 min at room temperature in the dark. Finally 100 µL of stop solution was added and the absorbance of each well was read at 450 nm. The unknown concentrations were read from the Ms TNF-α standard curve and multiplied by the dilution factors.

6.3 Results and Discussions

6.3.1 Synthesis of SAPE and structural validation of the synthesised compound by NMR and FTIR study

The reaction for the production of SAPE is shown in Fig 6.2. The 40:60 ethyl acetate:hexane mixture yielded the best results in terms of compound concentration. 13C NMR plot of the synthesized SAPE molecule is shown in Fig 6.3 and 1H NMR plot of the synthesized SAPE molecule is shown in Fig 6.4. FTIR plot of the synthesized SAPE molecule is shown in Fig 6.5. The data obtained are as follows: 13C (ppm): 3409, 65.8, 112.1, 118.1, 119.2, 126.12, 129.0, 130.1, 131.1, 135.2, 138.1, 161.8, 170.1. FTIR (cm^{-1}): 501, 672, 750, 1070, 1110, 1220,

1292, 1480, 1683, 3150. 1H (ppm): 3.1 (t, 2H), 4.52 (t, 2H), 6.7-6.98 (m, 2H), 7.1-7.48 (m,5H), 7.7-7.8 (m,2H), 10.7 (s,1H). The 3D structure of SAPE molecule is shown in Fig 6.6.

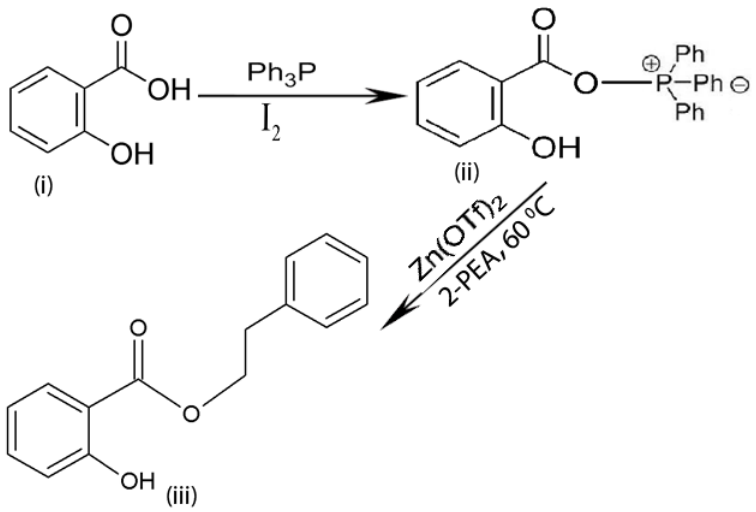

Fig 6.2: The reaction for the production of SAPE

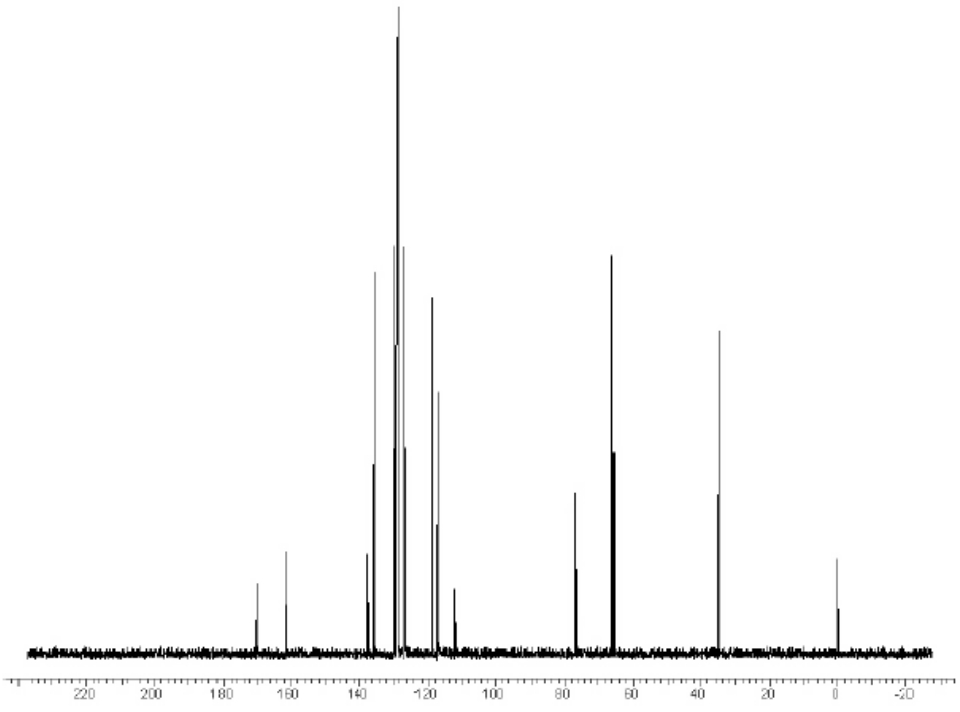

Fig 6.3 13C NMR of the synthesized SAPE molecule

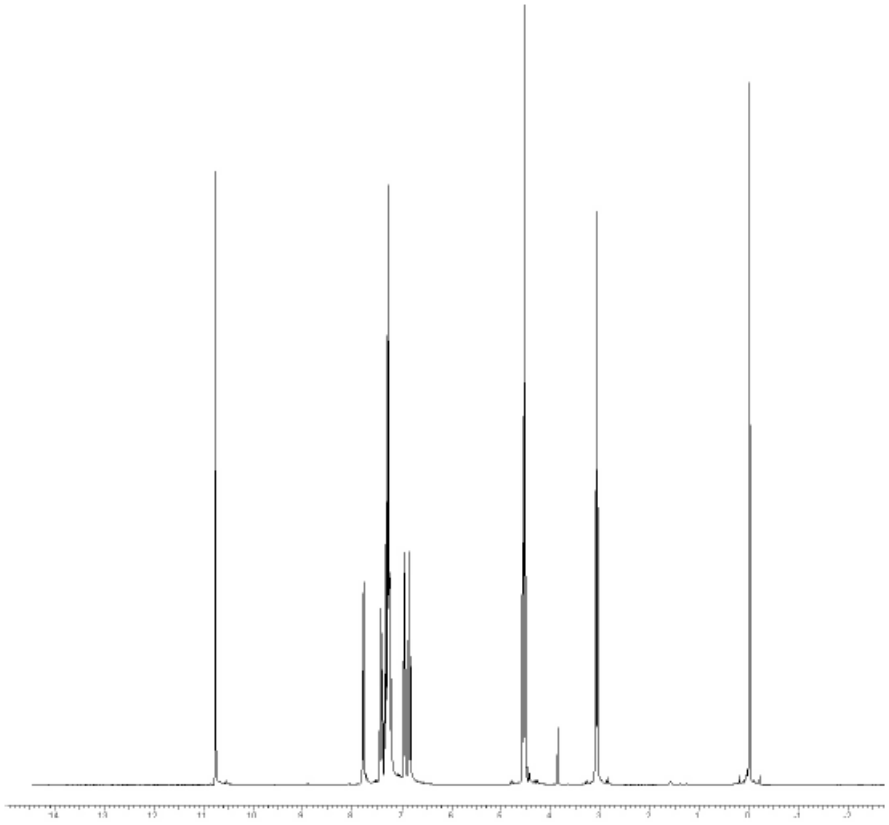

Fig 6.4 1H NMR of the synthesized SAPE molecule

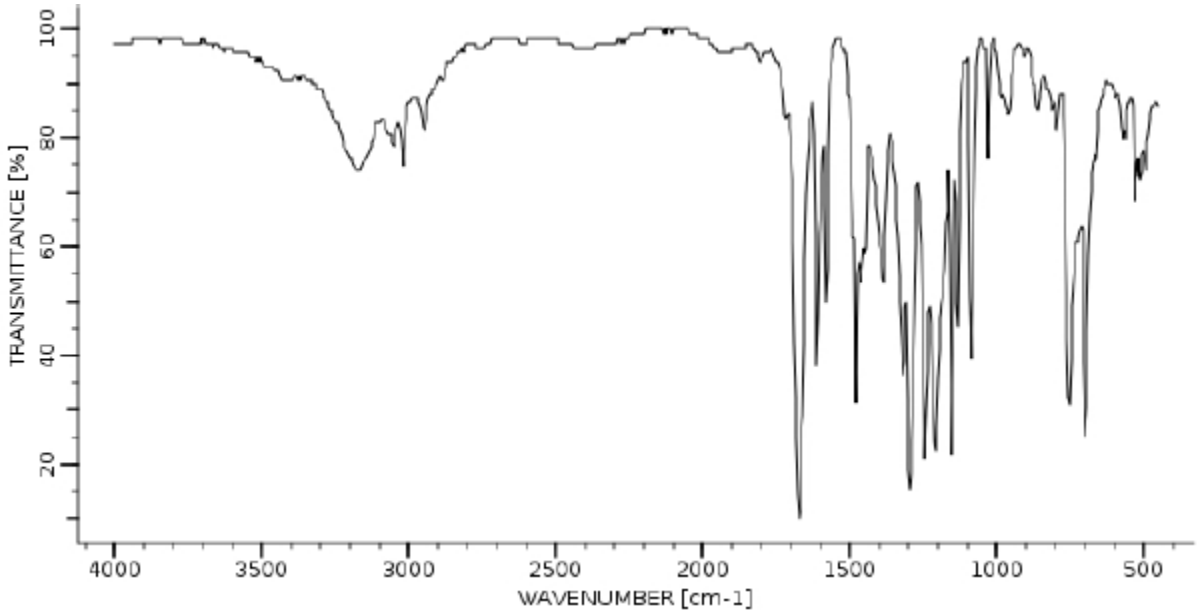

Fig 6.5 FTIR plot of the synthesized SAPE molecule

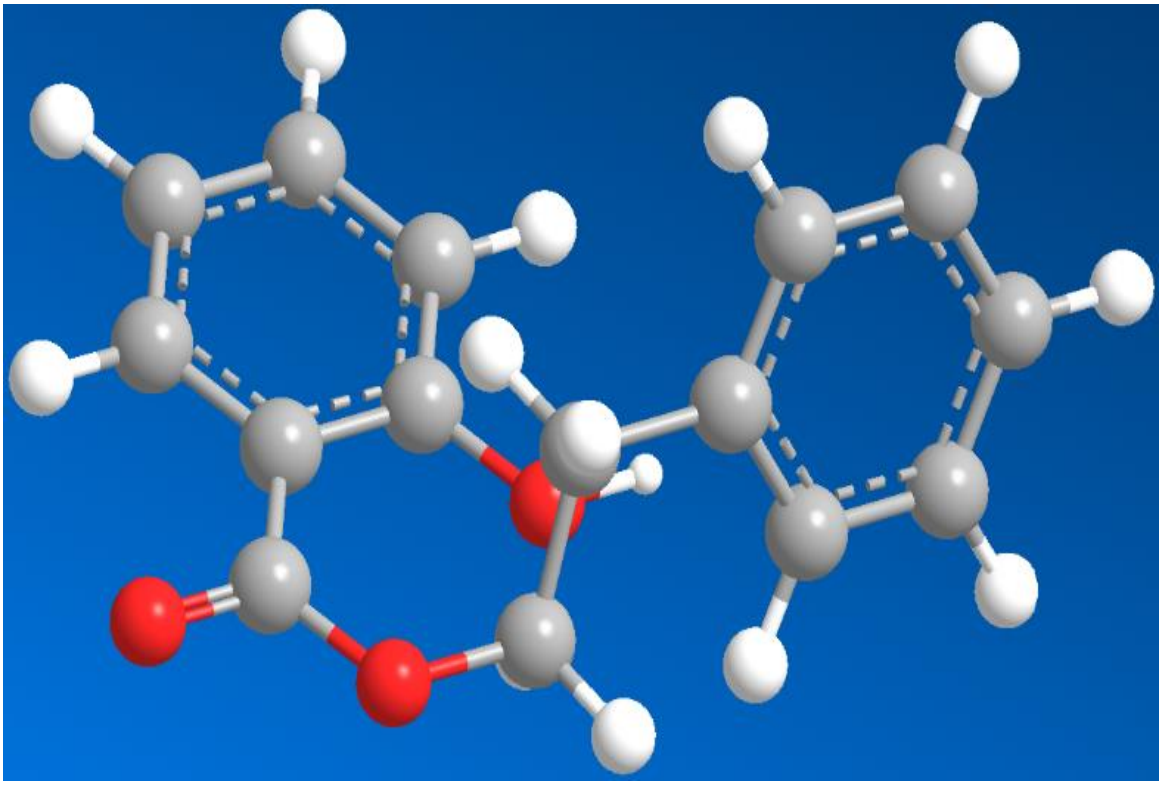

Fig 6.6 The 3D structure of SAPE molecule

6.3.3 *In silico* studies with SAPE and other anti-inflammatory drugs

6.3.3.1 Absorption, distribution, metabolism, and excretion (ADME) studies related to SAPE

Solubility, volume of distribution, absorption, blood brain barrier transport, bioavailability, health effects and LD_{50} values of SAPE molecule as predicted by ACD/Labs I-Lab 2.0 are shown in Table 6.3. ADME- toxicology study is an important step in the drug discovery process. An ideal oral drug should possess certain factors such as quick gastrointestinal tract absorption [24]. It was observed that the solubility (LogSw) was -4.03, while absorption (LogP) was 4.15, blood brain barrier transport (LogP) was 4.15 and volume of distribution was 0.44 L/kg. The maximum passive absorption was 100% from trancellular route, while permeability in human jejunum was 7.51×10^{-4} cm/s. The probability that the compound has bioavailability of %F (Oral) > 30% was 0.811and bioavailability of %F (Oral)

> 70% was 0. 358, whereas, the probability of effect on blood was 0.39; cardiovascular system 0.5; gastrointestinal system 0.6, kidney 0.26, liver 0.14 and lungs was 0.19. The LD_{50} values for rat were found to be 570 mg/kg (administered intraperitoneally) and 2500 mg/kg (administered orally). Hence it can be said that SAPE gets specifically distributed to its target, gets metabolized and removed in an appropriate manner without causing any damage. In the blood brain barrier prediction study, it was seen that the rate of brain penetration (LogPS) was -1.8, the extent of brain penetration (LogPB) was -0.2 and the brain/plasma equilibration rate [Log(PS*fu, brain)] was -3.1. It was thus found that the brain penetration of SAPE was sufficient for central nervous system (CNS) activity and this is shown by the compound as a green coloured square in the Fig 6.7, when compared to other known anti-inflammatory compounds (blue and orange coloured circles). The predicted physicochemical properties of SAPE viz. molar refractivity, molar volume, parachor, index of refraction, surface tension, density and polarizability and mass spectrometry related properties of SAPE are shown in Table 6.4. Moreover, the Lipinski-type properties were also deduced and were found to be favourable (Table 6.4). Hence this study predicted the nature of SAPE within an organism.

Table 6.3 Absorption, distribution, metabolism, and excretion (ADME) studies related to SAPE

Parameters	Activity of SAPE		
Solubility	LogSw (AB/LogSw 2.0): -4.03 Reliability: Moderate (RI = 0.69) Sw: 0.022 mg/ml		
Volume of distribution	Vd: 0.44 L/kg Acid (acid pKa<7.5 and no basic groups with pKa>6). Drugs in this group have small Vd values (95% of these values are less than 1L/kg).		
Absorption	Main physico-chemical determinants	LogP: 4.15 pKa (Acid): 3.70 pKa (Base): No pKa	
	Maximum passive absorption: 100%	Contribution from: Trancellular route = 100% Paracellular route = 0%	
	Permeability	Human jejunum scale (pH=6.5): Pe, Jejunum = 7.51×10^{-4} cm/s	
	Absorption rate	Ka = 0.051 min^{-1}	
Blood brain barrier transport	Main physico-chemical determinants	LogP: 4.15 pKa (Acid):3.7 Fraction unbound in plasma: 0.0335 pKa (Base): No pKa	
	BBB transport parameters	Rate of brain penetration: LogPS: -1.8 Extent of brain penetration: LogPB: -0.2 Brain/plasma equilibration rate: Log(PS*fu, brain): -3.1	
Bioavailability	Oral bioavailability between 30% and 70%	Probability that compound has: %F(Oral) > 30%: 0.811 %F(Oral) > 70%: 0.358	
	Positive for	Solubility, Stability (pH < 2), Passive absorption, First-pass metabolism, P-gp efflux	
Health effects	Probability of effect	Blood: 0.39; Cardiovascular system: 0.5; Gastrointestinal system: 0.6; Kidney:0.26 Liver: 0.14; Lungs: 0.19	
LD_{50} values	Species/Administration	LD50 (mg/kg)	Reliability (RI)
	Mouse/Intraperitoneal	610	Moderate(0.65)
	Mouse/Oral	2100	High(0.82)
	Mouse/Intravenous	85	Borderline(0.39)
	Mouse/Subcutaneous	380	Moderate(0.68)
	Rat/Intraperitoneal	570	Moderate(0.54)
	Rat/Oral	2500	Borderline(0.43)

Table 6.4 Physicochemical properties of SAPE

Physical properties		Lipinski-type properties		Mass spectrometry related properties	
Molar refractivity	71.85 ± 0.3 cm^3	Molecular weight	240.3	Monoisotopic mass	240.11503 Da
Molar volume	211.9 ± 3.0 cm^3	No. of hydrogen bond donors	1	Nominal mass	240 Da
Parachor	557.9 ± 4.0 cm^3	No. of hydrogen bond acceptors	2	Average mass	240.297 Da
Index of refraction	1.593 ± 0.02	TPSA	37.3	M+	240.114481 Da
Surface tension	47.9 ± 3.0 dyne/cm	No. of rotatable bonds	5	M-	240.115578 Da
Density	1.133 ± 0.06 g/cm^3			[M+H]+	241.122306 Da
Polarizability	28.48 ± 0.5 $10^{-24}cm^3$			[M+H]-	241.123403 Da
				[M-H]+	239.106656 Da
				[M-H]-	239.107753 Da

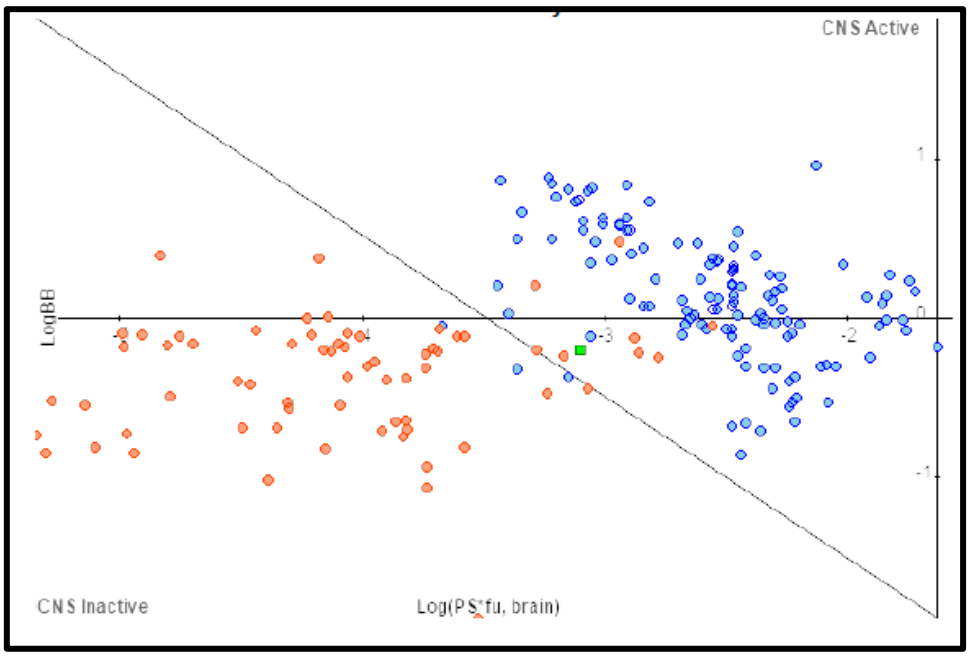

Fig 6.7 CNS activity of SAPE

6.3.3.2 Molecular docking study

Molecular docking predicts the preferred orientation of one molecule to a second one when bound to each other to form a stable complex. The strength of association or binding affinity between the two molecules based on the scoring functions (docking scores) is predicted based on the preferred orientation. In this instance, the protein can be can be assumed as a "lock" and the ligand as a "key" and molecular docking the optimization problem, which would describe the "best-fit" orientation of a ligand binding to a particular protein. An optimized conformation for both the protein and ligand and relative orientation between protein and ligand is obtained, whereby the free energy of the overall system is minimal.

A differential evolution algorithm is employed in MVD. The sum of the inter-molecular interaction energy between the ligand and the protein and the intra-molecular interaction energy of the ligand provided the solution to the algorithm. The modified piecewise linear potential (PLP) with new hydrogen bonding and electrostatic terms defines the energy scoring function [25,33,34]. The potential ligand binding site prediction employed was based on the hydrophobic pocket, and the algorithm used was a grid-based cavity prediction algorithm. It was seen that 0 % of lines hitting an inaccessible volume would only be possible

far from the protein as opposed to a value of 100 % corresponding to a binding site buried deeply in the protein. The cavities found were ranked according to their volume. The predicted potential ligand binding site (active site) displayed the cavity volume to be 56.32 $Å^3$, cavity surface of 175.36 $Å^2$ and positioned at X: 13.44; Y: 24.14; Z: 24.58 with a binding site radius of 15 A° (Fig 6.8).

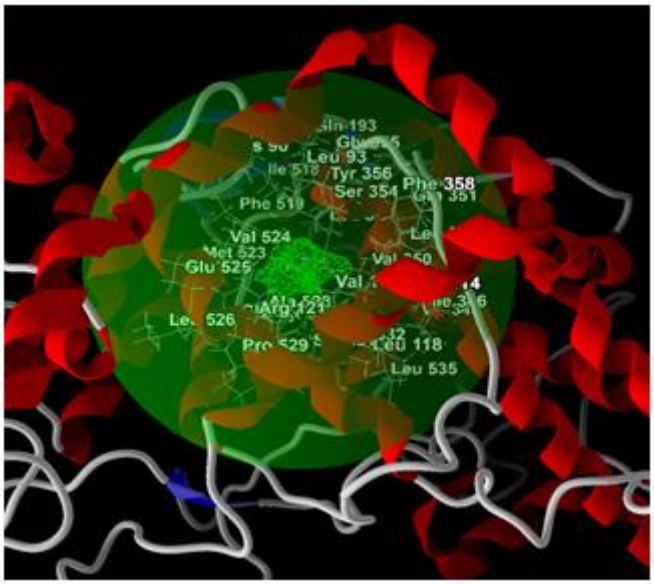

Fig 6.8 Predicted binding cavity of the COX-2 (PDB ID: 4PH9)

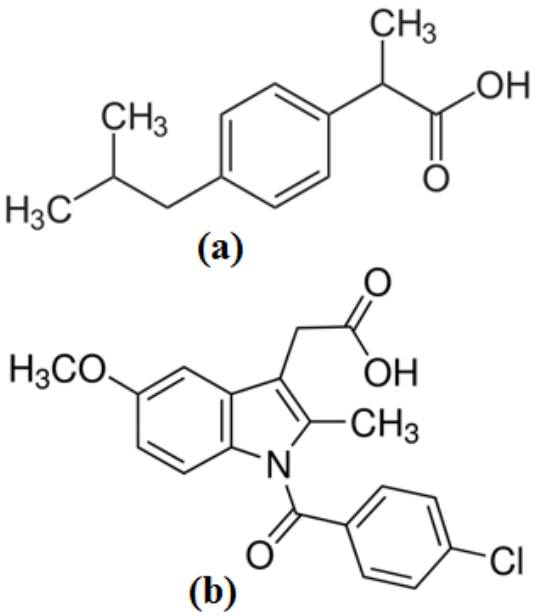

Fig 6.9 Structure of (a) Ibuprofen (b) Indometacin

The molecular docking simulation was performed against SAPE and two other established anti-inflammatory agents viz. ibuprofen and indometacin (Fig 6.9) for comparison using MVD 6.0. The sum of the inter-molecular interaction energy between the ligand and the protein and the intra-molecular interaction energy of the ligand provided the solution to the differential evolution algorithm. The docking energy scoring function was based on the modified piece-wise linear potential (PLP) which considered the new hydrogen bonding [25]. The docking solutions were evaluated using the MolDock Score [GRID], which is a grid-based scoring function. Moreover, MolDock SE was used as an alternative search algorithm since the compounds studied possessed several internal degrees of freedom [25]. The top poses which docked at the active site of COX-2 are shown in Fig 9 A and B, Fig 10 A and B and Fig 11 A and B. The values were ranked based on the Rerank score which is shown in Table 6.5.

Table 6.5 Docking scores of the compounds docked against COX-2

Name	MolDock Score[a]	Rerank Score [b]	Interaction[c]	Internal [d]	H-Bond[e]	MW	LE1[f]	LE3[g]
SAPE	-109.09	-94.57	-134.89	25.80	-2.26	240.30	-6.06	-5.25
Ibuprofen	-92.62	-77.50	-100.73	8.10	-4.33	205.27	-6.17	-5.17
Indometacin	-102.12	-84.89	-132.26	15.11	-5	357.78	-4.71	-3.39

Note: a - $E_{Score} = E_{inter}+E_{intra}$, where, E_{inter} is the ligand-protein interaction energy and E_{intra} is the internal energy of the ligand; b - The rerank score is a linear combination of E-inter between the ligand and the protein, and E-intra of the ligand weighted by pre-defined coefficients (more negative means more stable); c - The total interaction energy between the pose and the protein (kJ mol−1) (more negative means more stable); d - The internal energy of the pose.(The lesser the better); e - Hydrogen bonding energy (kJ mol−1). (more negative means more stable); f - Ligand Efficiency 1: MolDock Score divided by Heavy Atoms count. (more negative means more stable); g - Ligand Efficiency 3: Rerank Score divided by Heavy Atoms count. (more negative means more stable).

The favourable molecular docking scores for SAPE (Table 6.5) revealed that it can be docked at the active site of the COX-2 protein; thereby indicating that COX-2 usually favours SAPE compared to ibuprofen or indometacin. In the molecular docking engine, SAPE, ibuprofen, indometacin were ranked as the top five docking hits based on the MolDock score, Rerank score and interaction energy. The MolDock score employed in the present investigation is derived from the PLP scoring functions [33,34]. In the Table 6.5, E_{score} is the docking scoring function and is defined as: $E_{Score} = E_{inter}+E_{intra}$ (E_{inter} is the ligand-protein interaction energy and E_{intra} is the internal energy of the ligand). The Rerank score is a linear combination of E-inter (steric, Van der Waals, electrostatic and hydrogen bonding) between the ligand and the protein,

and E-intra (sp2–sp2, torsion, Van der Waals, electrostatic and hydrogen bonding) of the ligand weighted by the pre-defined coefficients.

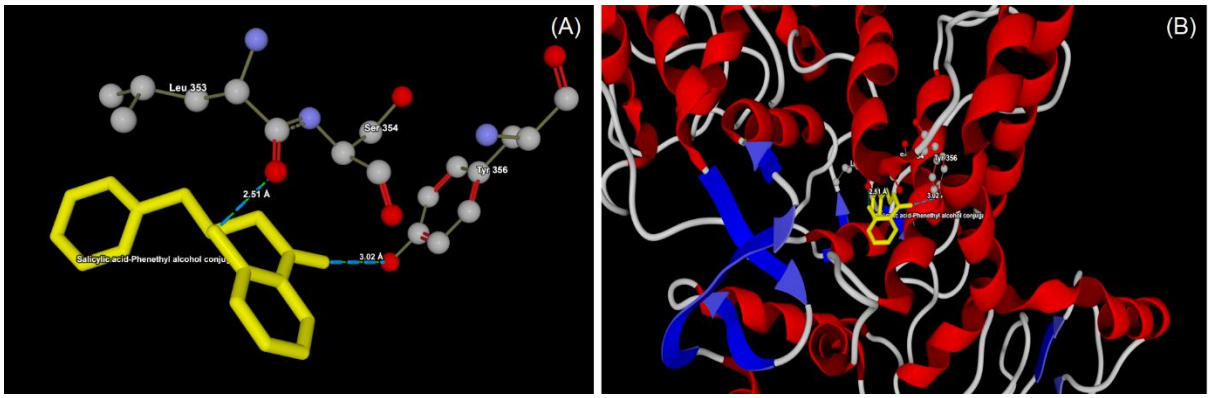

Fig 6.10 (A) Protein-ligand interactions between SAPE and active site residues of COX-2 enzyme. (B) Binding mode of SAPE at the active site residues of COX-2 enzyme

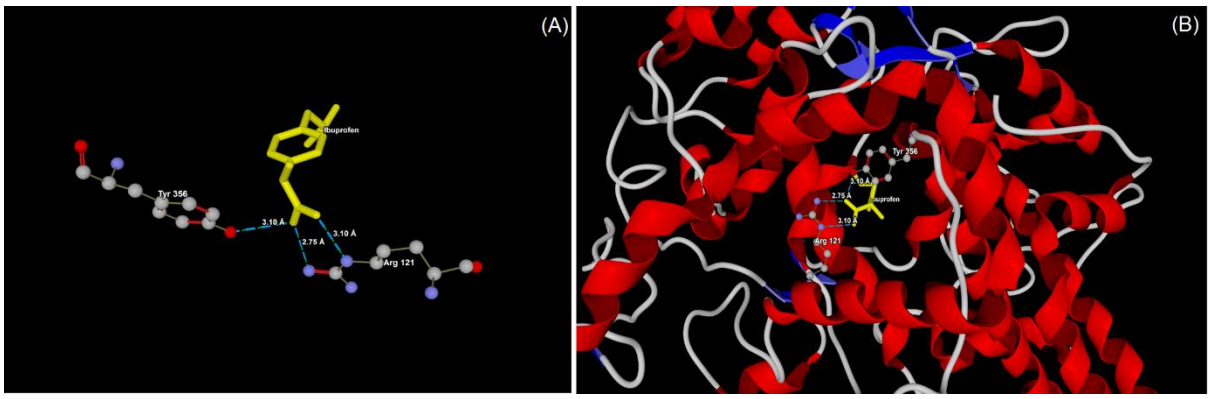

Fig 6.11 (A) Protein-ligand interactions between Ibuprofen and active site residues of COX-2 enzyme. (B) Binding mode of Ibuprofen at the active site residues of COX-2 enzyme

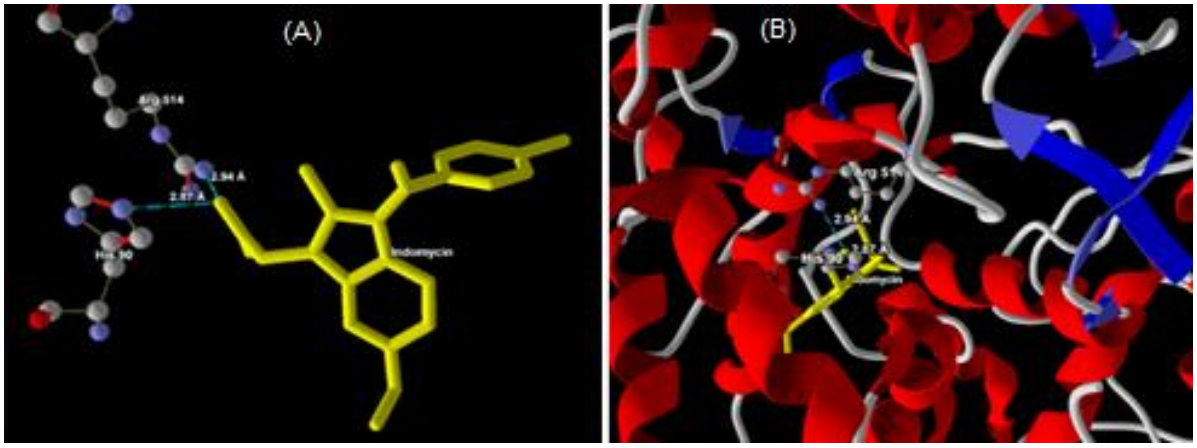

Fig 6.12 (A) Protein-ligand interactions between Indometacin and active site residues of COX-2 enzyme. (B) Binding mode of Indometacin at the active site residues of COX-2 enzyme

The molecular interactions were elucidated by the ligand-protein interaction analysis for the docking hits of SAPE, ibuprofen and indometacin using the MVD Ligand Energy Inspector. Table 6.6 shows the details of molecular interactions of the docking hits. The ligand–protein interaction, the residue interaction and their interaction distances were deduced. SAPE showed molecular interaction with Leu353(O) and Tyr356(OH) (Fig. 6.9 A and B), ibuprofen with Arg121(NH2) and Tyr356(OH) (Fig. 6.11 A and B) while indometacin with Arg514(NH) and His90(NE) (Fig. 6.12 A and B). The energy map and electrostatic interaction of the docking hits are shown in Fig. 6.13 A and B, Fig. 6.14 A and B and Fig. 6.15 A and B. The favourable molecular interaction is supported by the energy map of the enzyme, viz. favourable steric interaction (green colour), favourable hydrogen acceptor (turquoise colour), favourable hydrogen donor (yellow colour) and electrostatic interaction of the docked compounds.

Table 6.6 Molecular interaction analysis of the docked ligands with COX-2 enzyme

Compound	Interaction	Interaction energy	Interaction distance
SAPE	Leu353(O)---O(11)	-1.7	2.51 Å
	Tyr3556(OH)--- O(16)	-2.5	3.02 Å
Ibuprofen	Arg121(NE)---O(14)	-2.5	3.10 Å
	Arg121(NH2)---O(13)	-1.8	2.75 Å
	Tyr3556(OH)---O(13)	-2.5	3.10 Å
Indometacin	Arg514(NH)---O(3)	-2.5	2.94 Å
	His90(NE)---O(3)	-2.5	2.87 Å

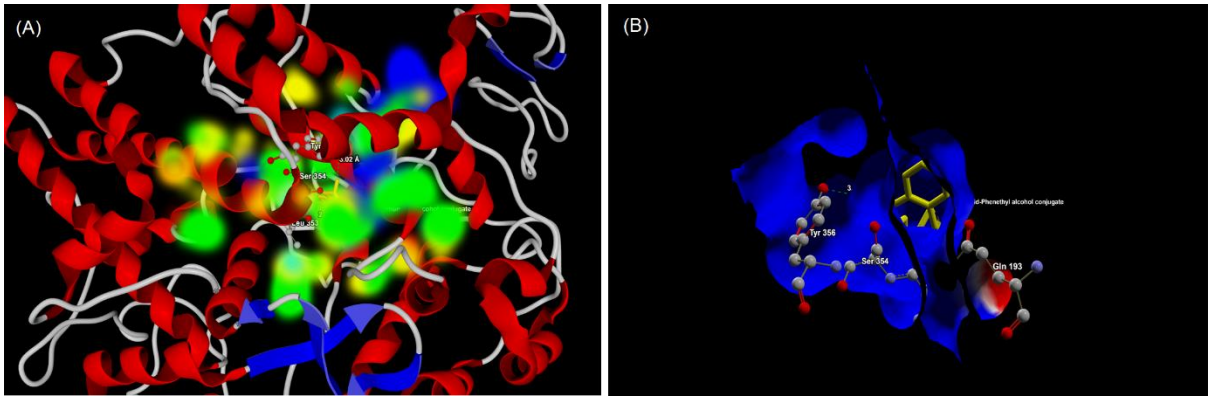

Fig 6.13 (A) Energy map of COX-2 interacting with SAPE depicting steric interaction favourable (green), hydrogen acceptor favourable (turquoise colour), hydrogen donor favourable (yellow colour) and electrostatic favourable (blue and red colour) regions. (B) Electrostatic interaction of SAPE at the enzyme active site indicating electronegative (blue) and electropositive regions (red).

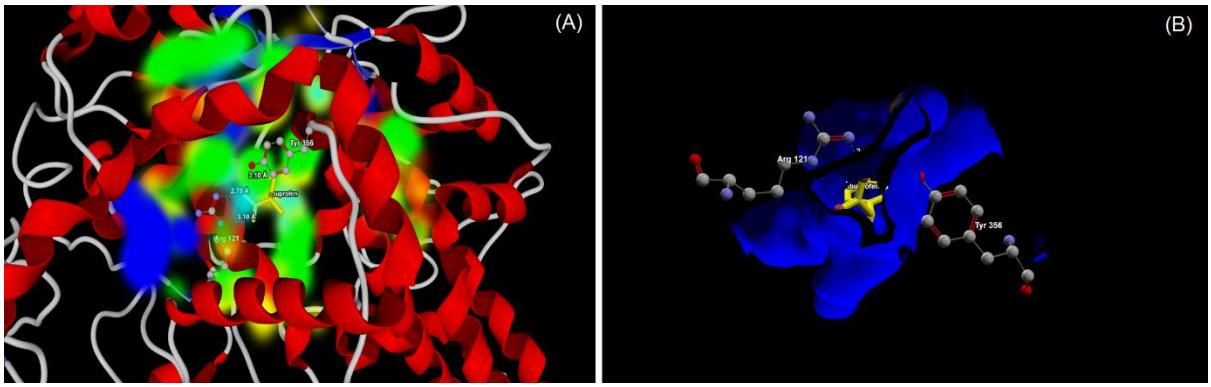

Fig 6.14 (A) Energy map of COX-2 interacting with Ibuprofen depicting steric interaction favourable (green), hydrogen acceptor favourable (turquoise colour), hydrogen donor favourable (yellow colour) and electrostatic favourable (blue and red colour) regions. (B) Electrostatic interaction of Ibuprofen at the enzyme active site indicating electronegative (blue) and electropositive regions (red).

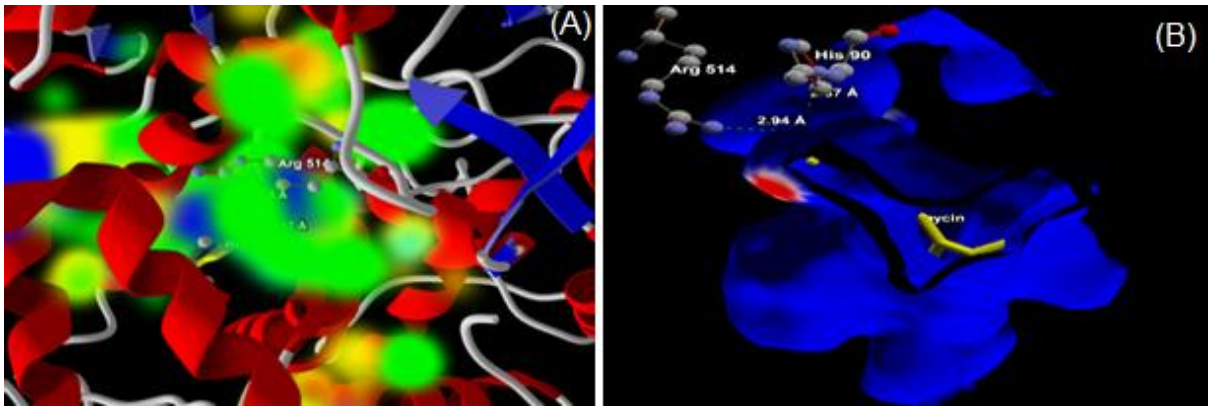

Fig 6.15 (A) Energy map of COX-2 interacting with Indometacin depicting steric interaction favourable (green), hydrogen acceptor favourable (turquoise colour), hydrogen donor favourable (yellow colour) and electrostatic favourable (blue and red colour) regions. (B) Electrostatic interaction of Indometacin at the enzyme active site indicating electronegative (blue) and electropositive regions (red).

6.3.3.3 Molecular dynamics simulation of protein-ligand docked complex

The MD simulation was conducted for the docking hits (SAPE-COX-2, ibuprofen-COX-2 and indometacin-COX-2 docked complexes). The RMSD data for the protein ligand docked complex of SAPE, ibuprofen and indometacin was plotted which is presented in Fig 6.16. The RMSD backbone of 20 ns MD simulations helped to understand the conformational changes of the protein-ligand binding complex and the protein occurring in the dynamic environment. The variations of the COX-2 protein and the protein-ligand binding complexes could be viewed in the RMSD plot. The average RMSD showed ~0.13 nm for the SAPE-COX-2 docked complex. While, the protein showed an average RMSD deviation of ~0.23 nm revealing more stable dynamic equilibrium condition of the protein-ligand complex. Thus, the conformational stability of the docked and the simulated complex during the 20 ns simulation run was observed.

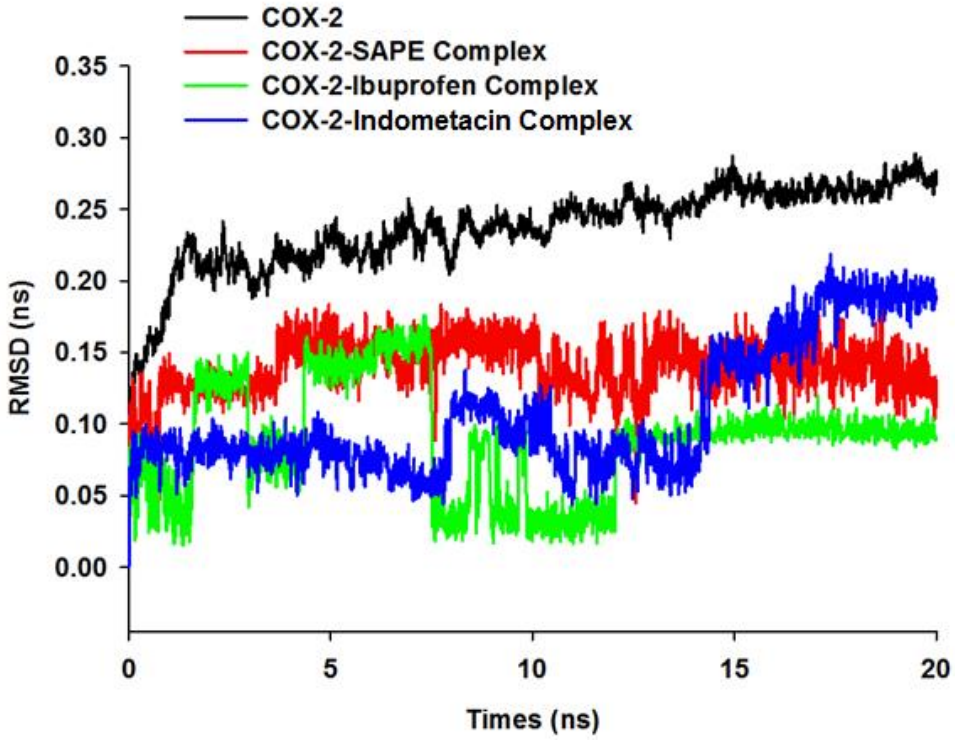

Fig 6.16 MD simulation showing the RMSD plot of the docked protein ligand complex showing that SAPE-COX-2 is more stable than the ibuprofen and indometacin complex

6.3.4 *In vitro* cytotoxicity of SAPE in animal cell line models

The membrane stability assay (Fig 6.17) was performed in erythrocytes with PBS, Triton X-100 and different concentrations (25, 50 and 100 µg/mL) of SAPE, and the results in

terms of percentage of haemolysis are shown in Fig 6.18. It was found to be 0.0704 % in case of the negative control PBS, and 100 % in case of the positive control Triton X-100. Whereas, in case of SAPE it was found to be 58.08 % for 25 µg/mL, which differed significantly at $p \leq 0.01$ with the positive control; and 56.28 % and 54.88 % for 50 µg/mL and 100 µg/mL respectively, with significant difference ($p \leq 0.001$) with the positive control . Hence it was seen that up to the studied concentrations, the surface functionalization of SAPE conferred stability to the red blood cells and prevented haemolysis to a considerable extent. It was also observed that the membrane stability increased with increasing concentration of SAPE. Triton X-100 is generally used to lyse cells or to permeabilize the membranes of living cells. It was observed that in presence of SAPE, Triton X-100 exhibited significantly less haemolysis than the pristine samples.

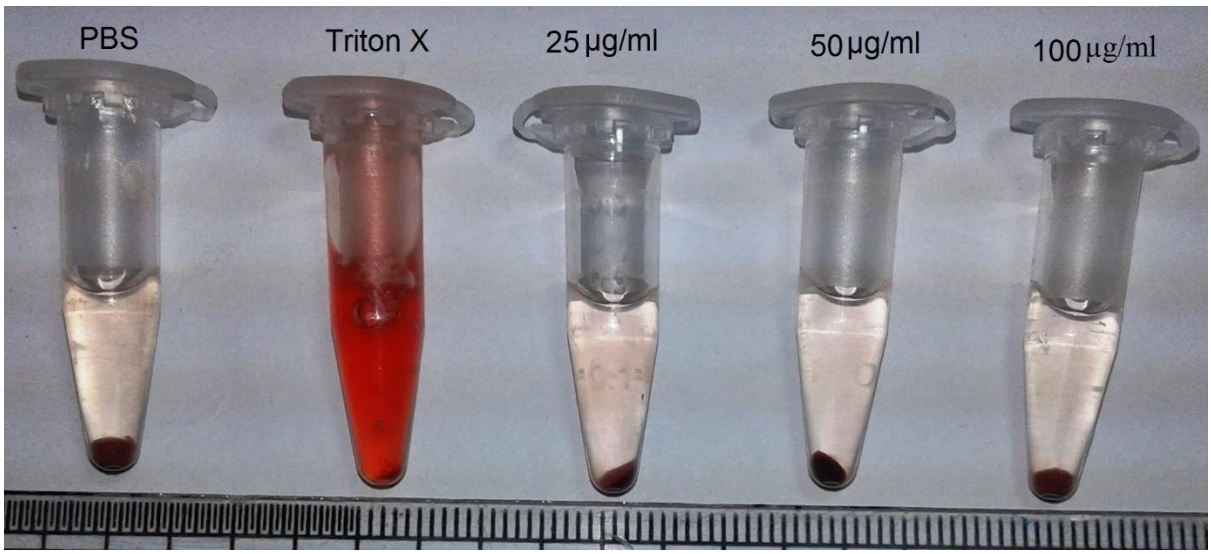

Fig 6.17 Photograph of membrane stability assay in erythrocytes with PBS, Triton X and different concentrations (25, 50 and 100 µg/ml) of SAPE

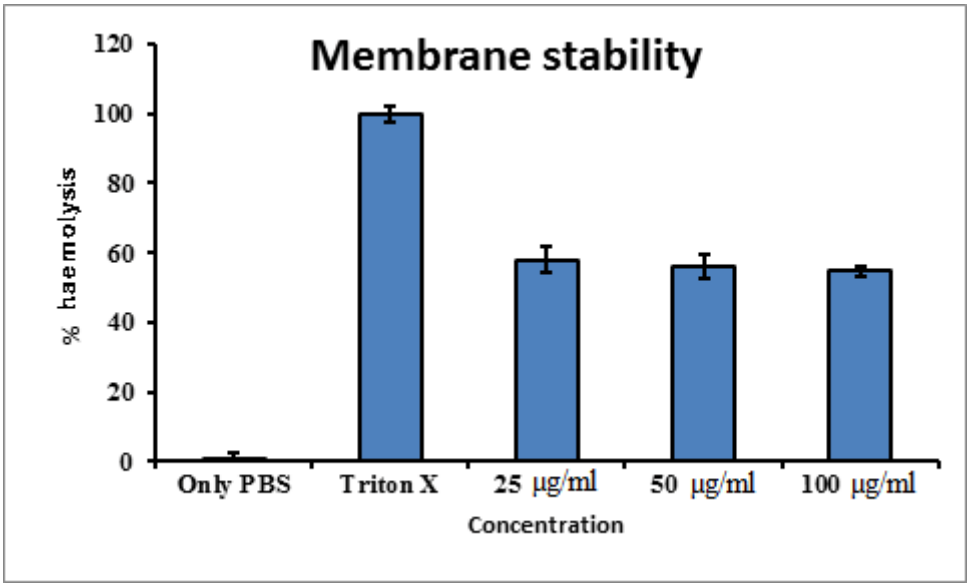

Fig 6.18 Membrane stability assay of SAPE in erythrocytes

MTT is yellowish in colour and the mitochondrial dehydrogenase of viable cells cleave the tetrazolium ring, yielding purple insoluble formazan crystals, which are dissolved in a suitable solvent [35]. The MTT assay of SAPE was performed with PBMC and the results are shown in Fig 6.19. It was seen that there was no any significant change ($p \leq 0.05$) in the number of viable cells after being treated with 25, 50 and 100 µg/mL of SAPE, as compared to the control.

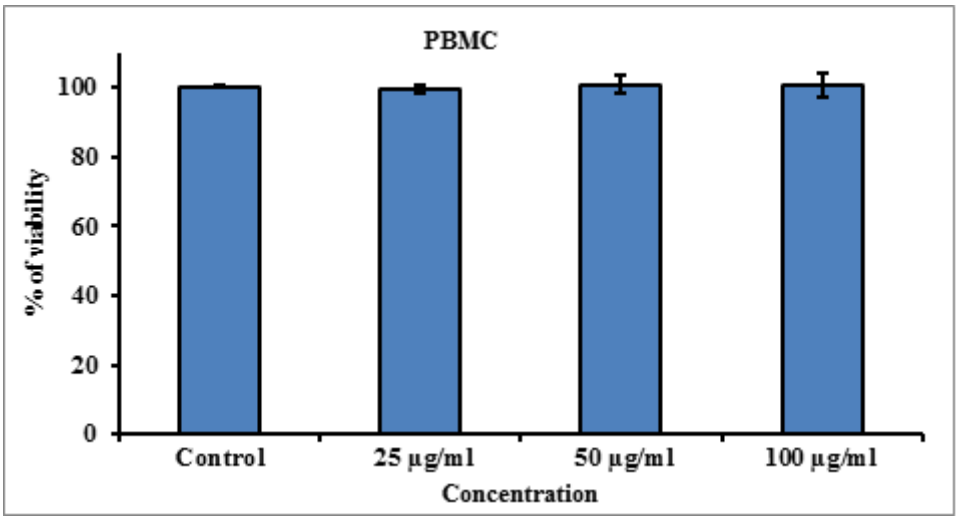

Fig 6.19 Results of MTT assay of SAPE in PBMC

HepG2 is a popularly available and well characterized liver cancer cell line which is frequently employed in *in vitro* studies as experimental model. It is extensively used as a

cellular reference model in pharmaceutical studies involving development of new drugs and studies pertaining to their metabolism and enzymes involved in the drug's inhibition or induction potential. HepG2 also expresses most of the drug-metabolising enzymes [36]. The HepG-2 cells (Fig 6.20) were treated with different concentrations (control, 25, 50, 100 and 200 µg/mL) of SAPE, and the MTT assay was performed, whose results are shown in Fig 6.21. Even though the percentage of viable cells decreased with increasing concentrations of SAPE, it was seen that there was no any significant change ($p \leq 0.05$) in the number of viable cells after being treated with varying concentrations of SAPE, as compared to the control.

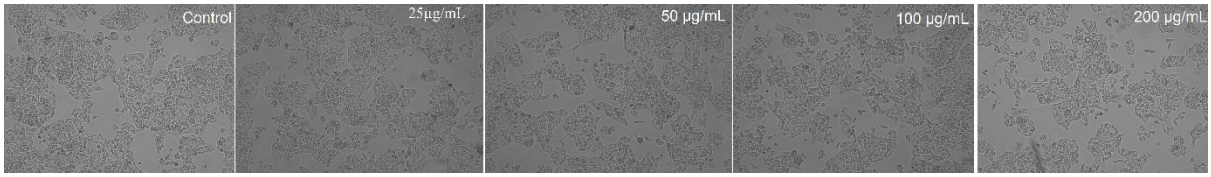

Fig 6.20 Treatment of HepG-2 cells with different concentrations (control, 25, 50, 100 and 200 µg/ml) of SAPE

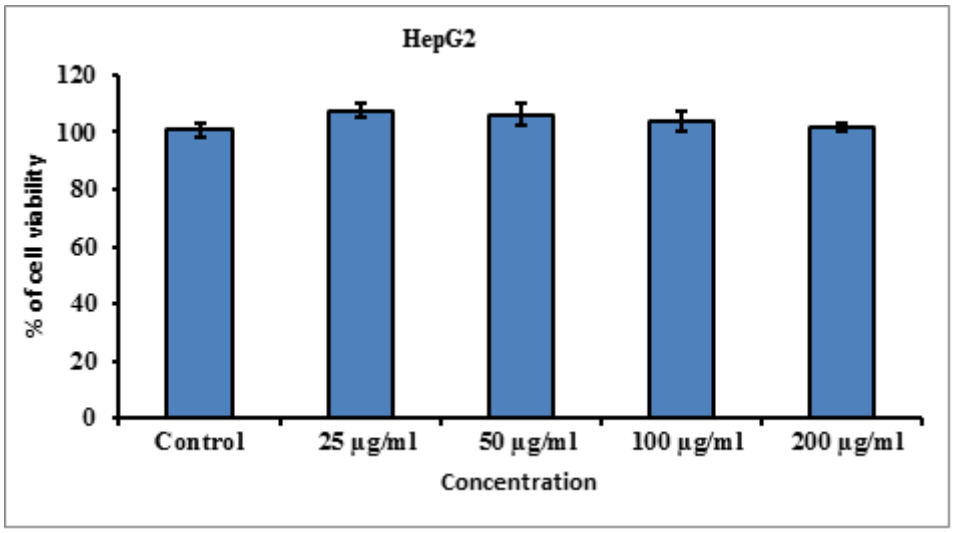

Fig 6.21 Results of MTT assay of SAPE in HepG-2 cells

Caco-2 is a human intestinal cell line derived from a colon carcinoma and is extensively used as a model of the intestinal barrier. In culture it undergoes a process of spontaneous differentiation leading to the formation of a monolayer of cells. It also expresses several morphological and functional characteristics of the mature absorptive enterocytes with brush border layer as found in the small intestine. It is thus used to measure interaction, uptake and cellular transport of drugs and food components [37,38]. The CaCo-2 cells (Fig 6.22) were treated with different concentrations (control, 25, 50, 100 and 200 µg/mL) of SAPE, and the MTT assay was performed, whose results are shown in Fig 6.23. It was seen that the

percentage of viable cells increased with increasing concentration of SAPE. There was no any significant change in the number of viable cells after being treated with 25, 50 and 100 µg/mL of SAPE, as compared to the control. However at 200 µg/mL of SAPE a significant difference ($p \leq 0.05$) was observed.

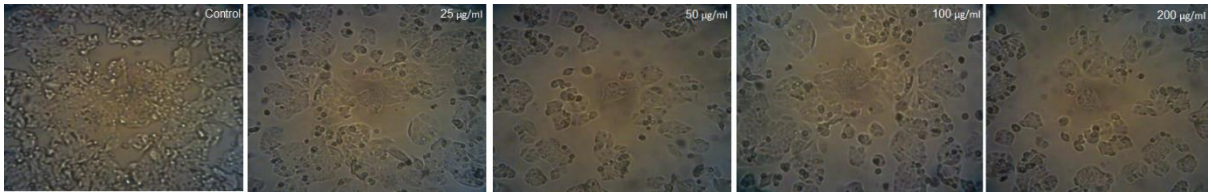

Fig 6.22 Treatment of CaCo-2 cells with different concentrations (control, 25, 50, 100 and 200 µg/ml) of SAPE

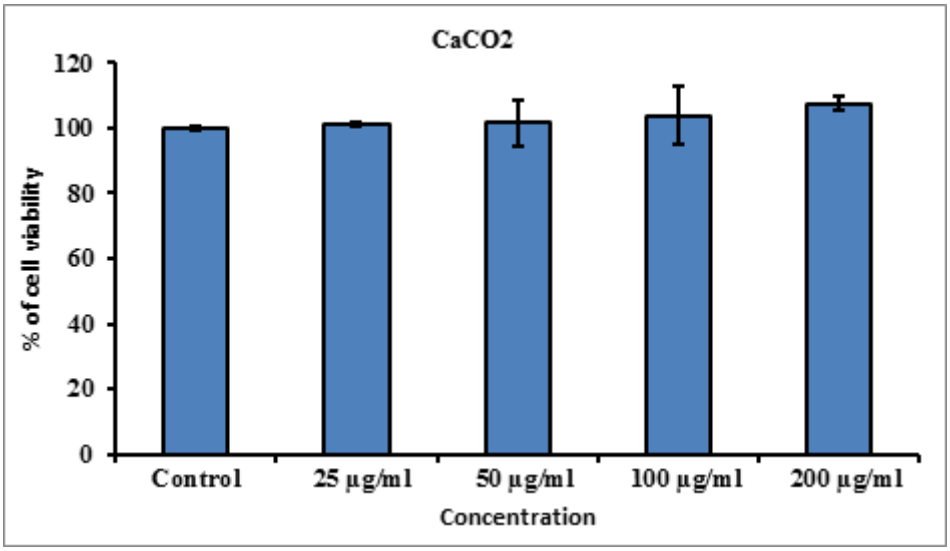

Fig 6.23 Results of MTT assay of SAPE in CaCo-2 cells

Alamar Blue® is a water-soluble dye which is extremely stable and nontoxic to cells. The Alamar Blue® assay is sometimes considered superior MTT test as continuous monitoring of cultures over time is possible [39]. It is radioisotopes free, extraction free, and has versatility detection with excellent reproducibility and sensitivity [40]. The Alamar Blue® assay was performed on CaCo-2 cells with different concentrations (control, 25, 50, 100 and 200 µg/mL) of SAPE and the results are shown in Fig 6.24. It was seen that there was no any significant change ($p \leq 0.05$) in the number of viable cells after being treated with varying concentrations of SAPE, as compared to the control. However the percentage of viable cells increased up to 105.74 % for 50 µg/mL and henceforth decreased increasing concentration of SAPE.

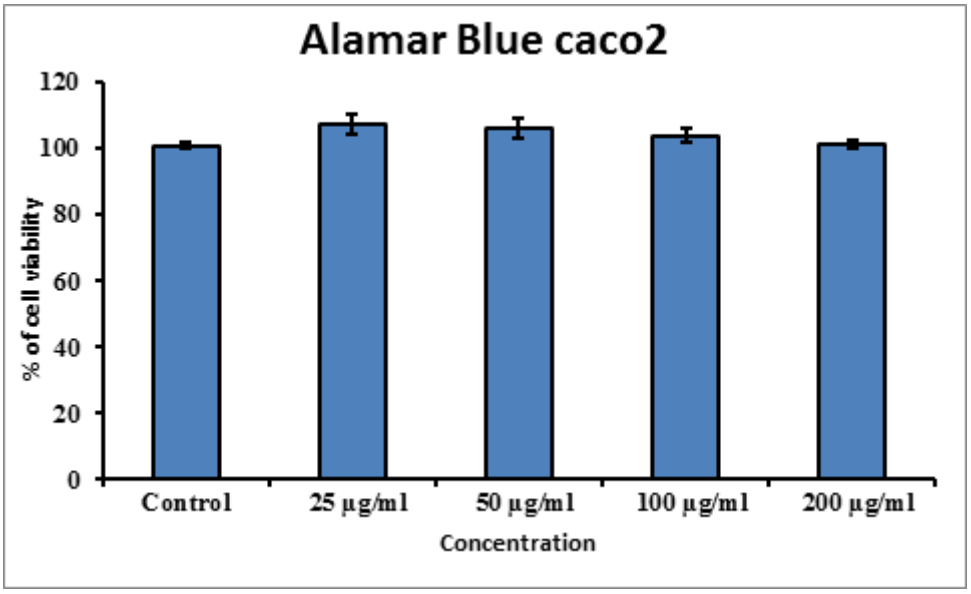

Fig 6.24 Results of Alamar Blue® assay of SAPE in CaCo-2 cells

6.3.5 *In vivo* study for anti-inflammatory role of SAPE in animal model

6.3.5.1 Pre-test in paw oedema model

The carrageenan induced rat paw oedema model is a model of acute inflammatory process. Initially during the first hour after carrageenin injection, histamine, serotonin and bradykinin are released, followed by the release of prostaglandins at around the third hour. This process lasts for about six hours post injection. This method is commonly used to evaluate the effect of NSAIDs that primarily acts inhibitors of COX enzyme involved in prostaglandins synthesis [41]. The results obtained for the paw oedema model are shown in Table 6.7. A decrease in the % of paw oedema was observed in the SAPE treated group right from the 1st till the 5th hour. However, significant difference was observed only in the 3rd, 4th and 5th hour after carrageenan injection. This difference after the 3rd hour may be indicative that the action of SAPE involves the inhibition of the synthesis or the release of prostaglandins. The absence of significant difference in the early hours may be due to the lack of influence of SAPE on the early mediators, viz., histamine, serotonin or bradykinin

Table 6.7 Effect of SAPE on the carrageenan induced paw oedema model

Treatment	% of oedema at different time after carrageenan injection				
	1h	2h	3h	4h	5h
Control	30.97±2.25	26.33±3.11	26.67±2.26	22.61±2.51	20.34±2.22
SAPE	29.63±2.99	25.32±2.41	18.59±3.09*	16.94±3.44*	11.59±3.14*

Results in mean±SD (n=4). * Differ significantly from the control group ($p \leq 0.05$)

6.3.5.2 Change in body weight of the different groups of rats and evaluation of disease activity index (DAI)

After the treatment of NSAIDs weight loss may occur. This weight loss may result mostly from cachexia, the major cause of which may be due to cytokine excess [42]. However, as seen in Fig 6.25, a steady increase in the percentage of body weight with time was observed in all the three groups. The increase was however higher in the control group as compared to the SAPE treated and indometacin treated groups.

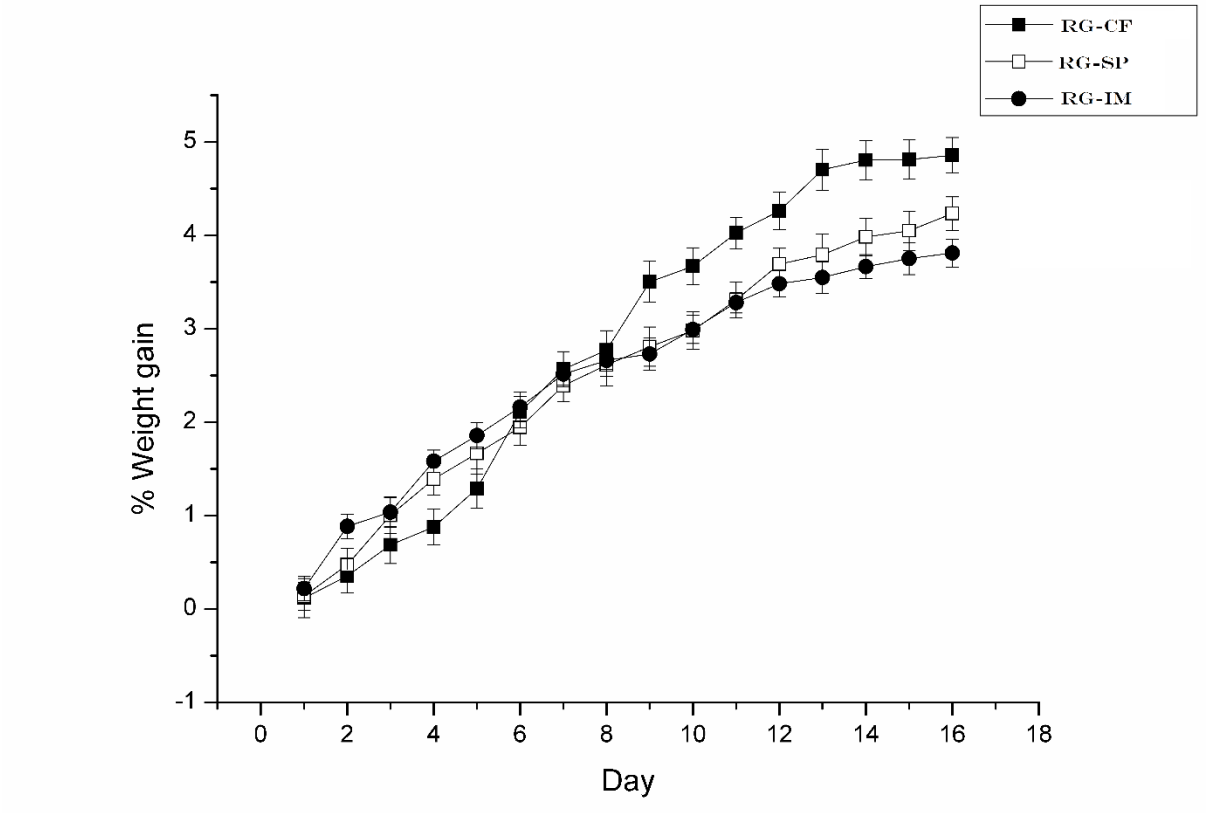

Fig 6.25 Change in body weight of the different groups of rats (RG-CF: control without any treatment; RG-SP: treated with SAPE; RG-IM: treated with indometacin) until the day of induction of colitis

The inflammatory bowel diseases (IBDs) like Crohn's disease (CD) and ulcerative colitis (UC) are marked using the disease activity index (DAI) which help to evaluate disease

activity at a given time [43]. The disease activity index scores of the different treatment groups of rats are shown in Table 6.8. It was seen that the colitis induced group without any treatment (RG-CI) marked the highest score for DAI with 2.42, whereas in the control group it was 0. Both the SAPE (1.04 DAI) and indomethacin (0.92 DAI) treated groups recorded lower scores than the RG-CI group. Hence there was a marked difference in the degree of induced disease after the rat models underwent pre-treatment with SAPE.

Table 6.8 Disease activity index scores of the different group of rats

	RG-CI	RG-CF	RG-SP	RG-IM
DAI	2.42	0	1.04	0.92

Note: Results are mean of 8 readings

6.3.5.3 Scanning electron microscope (SEM) study of intestinal morphological changes

Excised intestines of the different groups of rats after treatment and euthanization are shown in Fig 6.26. SEM image of the intestinal section from RG-CF, RG-CI, RG-SP and RG-IM rat groups are shown in Fig 6.27, 6.28, 6.29 and 6.30 respectively. Certain degree of tissue damage and rupture was observed in the colitis induced groups (RG-CI, RG-SP and RG-IM), which was not seen in the control group. As compared to the colitis induced group without any treatment, the SEM images for the SAPE and indomethacin treated groups displayed distinctive reduction in the level of tissue damage. This clearly indicates a reduction in the level of reduction of colitis after treatment with SAPE.

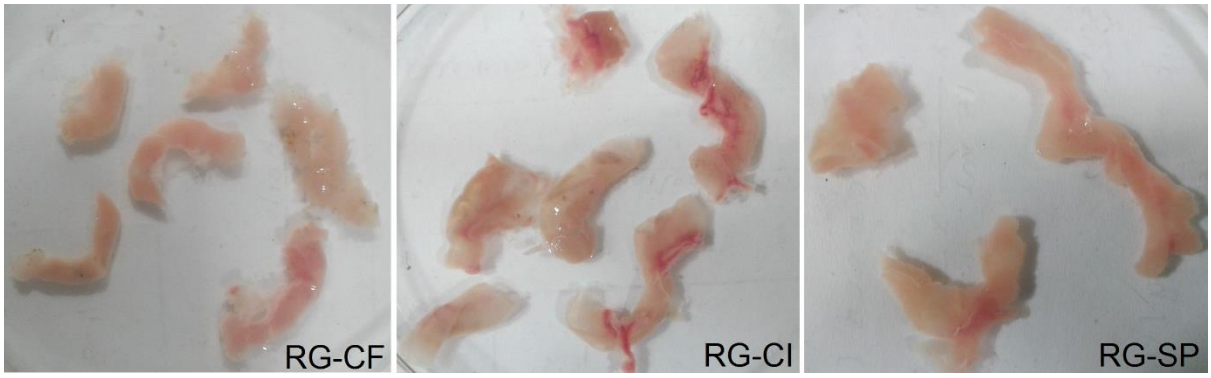

Fig 6.26 Excised intestines of the different groups of rats after treatment and euthanization (RG-CF: colitis free control group without any treatment; RG-CI: colitis induced group without any treatment; RG-SP: colitis induced group treated with SAPE)

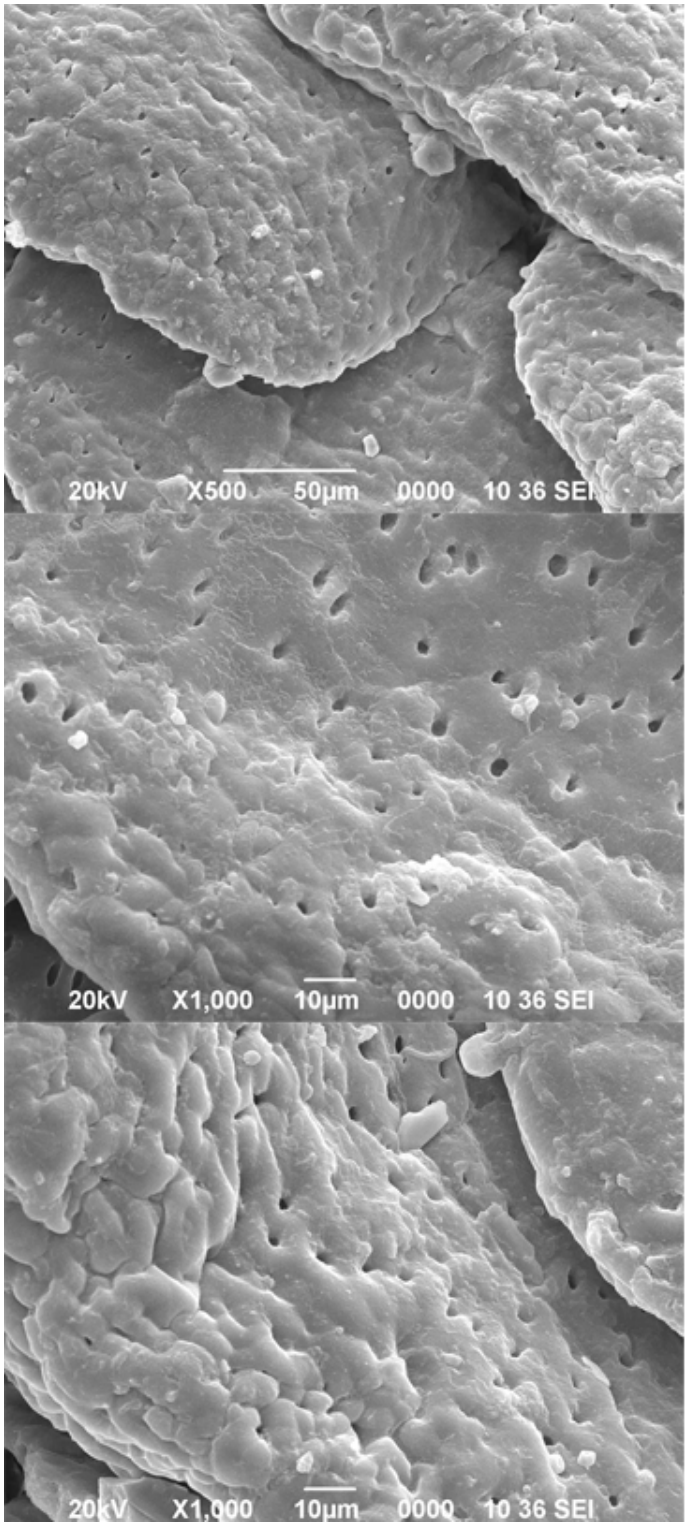

Fig 6.27 SEM image of the intestinal section from RG-CF (colitis free control group without any treatment) rats

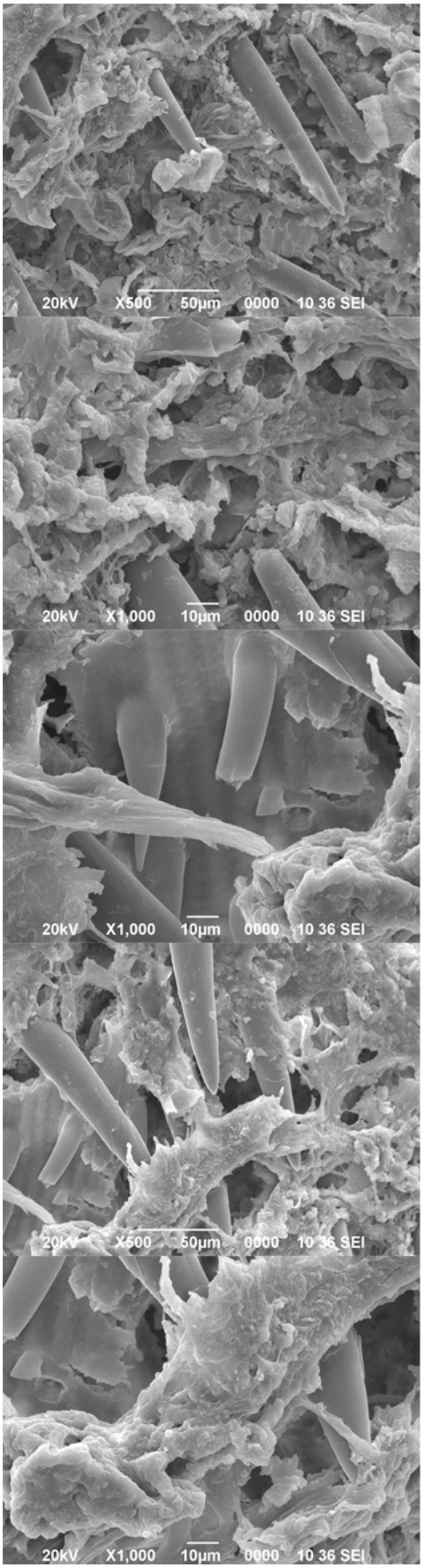

Fig 6.28 SEM image of the intestinal section of RG-CI (colitis induced group without any treatment) rats

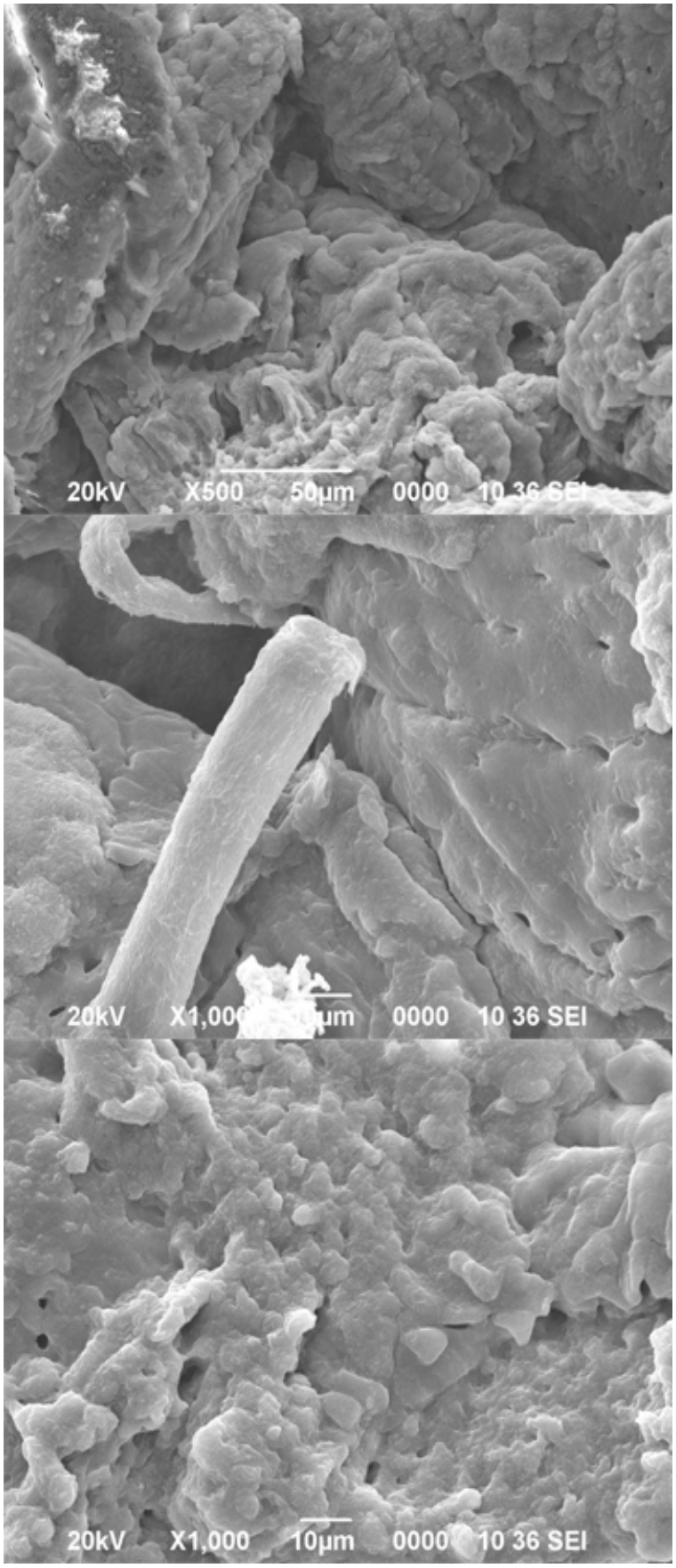

Fig 6.29 SEM image of the intestinal section of RG-SP (colitis induced group treated with SAPE) rats

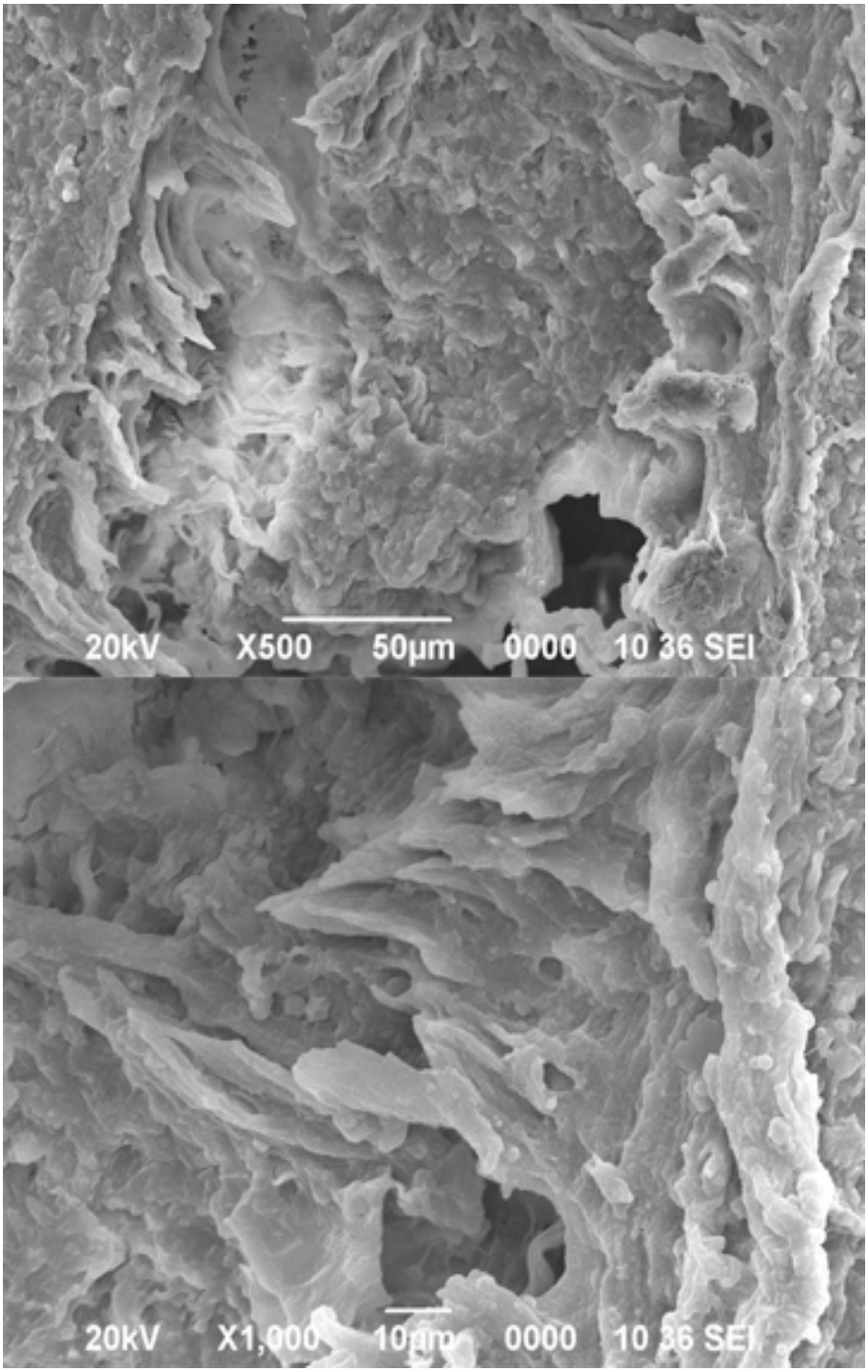

Fig 6.30 SEM image of the intestinal section of RG-IM (colitis induced group treated with indometacin) rats

6.3.5.4 Antioxidative and anti-inflammatory role of SAPE on animal model

Inflammation is a defence mechanism in which leucocytes migrate from the vasculature into damaged tissues to destroy the agents responsible for causing tissue injury. Inflammation may be acute or chronic. Acute inflammation is a limited beneficial response during an infectious challenge, whereby neutrophilic leucocytes infiltrate initially, but monocytic cells predominate after 24 to 48 hours. As a result of this, tissue damage at the site of inflammation due to the accumulation of neutrophil-secreted proteases and reactive oxygen species is prevented. During these inflammatory disorders, the concentrations acute phase plasma proteins increase (positive acute phase proteins) or decrease (negative acute phase proteins) by at least 25 %. In contrast, chronic inflammation is a persistent phenomenon that can lead to tissue damage. It is histologically associated with the presence of mononuclear cells, such as macrophages and lymphocytes [44]. The cytokines are stimulators of the production of acute phase proteins that are produced during inflammatory processes. These inflammation associated cytokines include interleukin-6 (IL-6), IL-1β, tumour necrosis factor-α (TNF-α), interferon-γ, transforming growth factor-β, IL-8, colony-stimulating factors and growth factors. Functional pleiotropy and redundancy are characteristic features of these cytokines [44,45]. On the other hand, inflammation induced oxidative damage is aggravated by the decrease in antioxidant enzymes activities such as catalase (CAT), glutathione S-transferase (GST) and gamma-glutamyl transferase (GGT) which acts as free radical scavengers in conditions associated with oxidative stress [46]. Oxidants such as free radicals, or sometimes nonradical species like enzymes, attack lipids containing C-C double bond(s) that involve hydrogen abstraction from a carbon and insertion of oxygen resulting in lipid peroxyl radicals and hydroperoxides. This phenomenon is known as lipid peroxidation. The polyunsaturated fatty acids (PUFAs), glycolipids, phospholipids (PLs), and cholesterol (Ch) are well-known targets of peroxidative modification [47] and the most common targets are components of biological membranes [48]. Lipid peroxidation produces a wide variety of secondary oxidation products, like the aldehydes, among which malondialdehyde (MDA) is the most mutagenic [47].

6.3.5.4.1 Antioxidative effects

MDA is a three-carbon, low-molecular weight aldehyde that is generated as an end-product by decomposition of arachidonic acid and larger PUFAs, through enzymatic or

nonenzymatic processes. MDA is highly reactive and toxic and reacts with multiple biomolecules such as proteins or DNA that leads to the formation of adducts. Excessive MDA production has been associated with different pathological states and subjects affected by several diseases have increased levels of MDA. Hence, it is used as a convenient biomarker for lipid peroxidation by its facile reaction with thiobarbituric acid (TBA) [47,48]. Results of assay for malondialdehyde (MDA) content in the intestinal tissue extract for different treatment groups of rats are shown in Fig 6.31. It was seen that there was significant difference ($p \leq 0.05$) in the content of MDA among all the groups. The colitis induced group without any treatment showed the highest content (0.26 pg/ul), while the content was less in the SAPE treated group (0.10 pg/ul) as compared to the indomethacin treated group (0.16 pg/ul). Hence, SAPE can be considered as a potent inhibitor of lipid peroxidation in inflamed tissues.

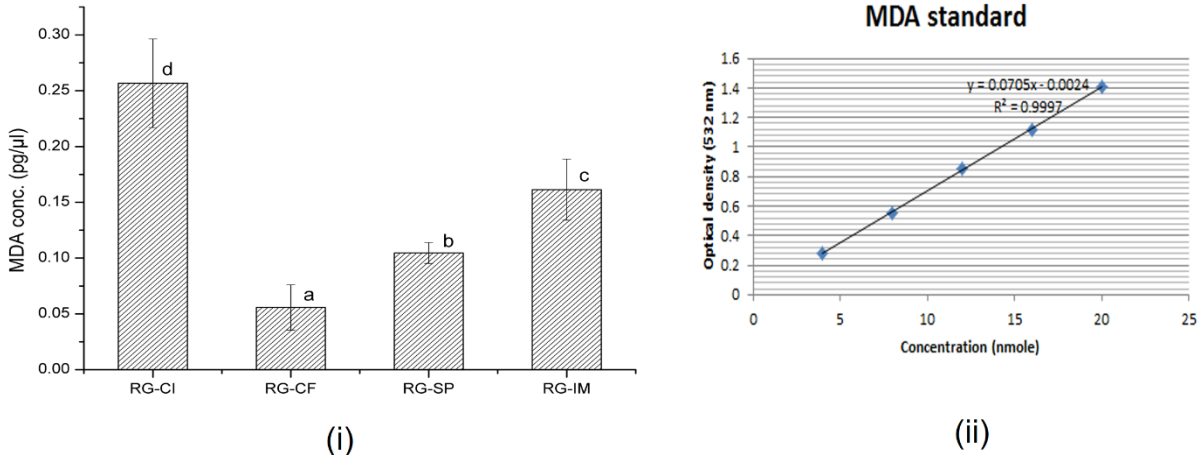

Fig 6.31 Results for assay of malondialdehyde (MDA) content in the intestinal tissue extract for different treatment groups of rats (RG-CI: colitis induced group without any treatment; RG-CF: colitis free control group without any treatment; RG-SP: colitis induced group treated with SAPE; Group RG-IM: colitis induced group treated with indometacin)

Catalase (CAT) enzyme is a primary antioxidant defence component to protect cells them from oxidative stress as it eliminates hydrogen peroxide ($2H_2O_2 \rightarrow 2H_2O + O_2$). H_2O_2 is a non-radical reactive oxygen species which is toxic to cells but is also permeable to cell membranes and directly inactivate few enzymes. In extracellular environment, H_20_2 generates highly reactive hydroxyl radicals ($^{\cdot}OH$) by reaction with transition metals like iron and copper. CAT is considered as a sensitive biomarker of oxidative stress in cells and high activity is usually marked in liver tissues [46,49]. Results of assay for catalase (CAT) concentration in the intestinal tissue extract for different treatment groups of rats are shown in Fig 6.32. It was seen that there was significant difference ($p \leq 0.05$) in the content of CAT among all the groups.

The colitis induced group without any treatment showed the lowest content (35.25 mU/mL), while the control group recorded the highest content (201.25 mU/mL). The content was again higher in the SAPE treated group (168.75 mU/mL) as compared to the indomethacin treated group (152.00 mU/mL), thus indicating a positive role of SAPE in the synthesis and activity of the antioxidative enzyme CAT.

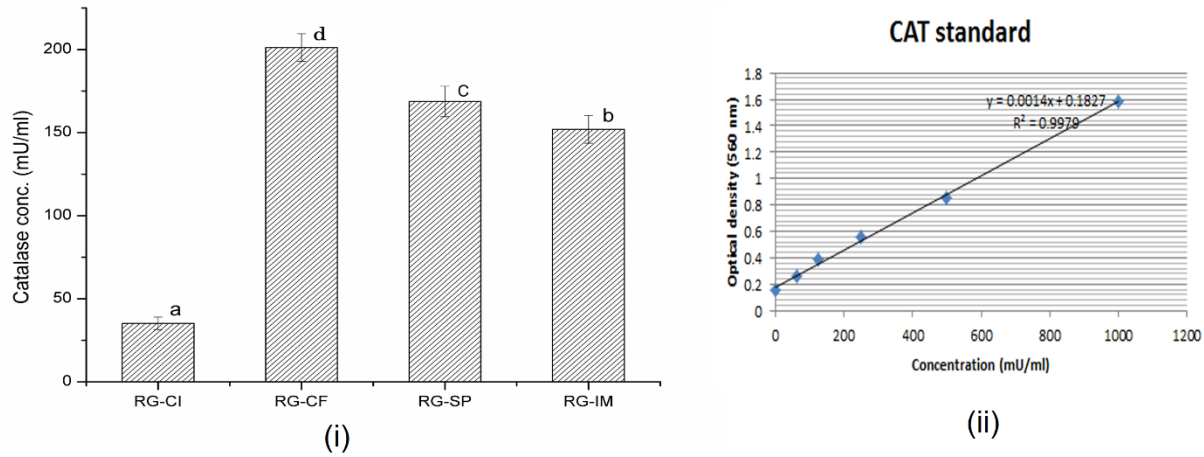

Fig 6.32 Results for assay of catalase (CAT) concentration in the intestinal tissue extract for different treatment groups of rats (RG-CI: colitis induced group without any treatment; RG-CF: colitis free control group without any treatment; RG-SP: colitis induced group treated with SAPE; Group RG-IM: colitis induced group treated with indometacin)

Gamma-glutamyl transferase (GGT) is a glycosylated cell-surface enzyme that is partially embedded in the outer surface of the plasma membrane at the N-terminal transmembrane domain. It is normally present in the serum being carried primarily with lipoproteins and albumin, which are active in the liver, intestine proximal renal tubule and pancreas [50,51]. GGT contributes to the extracellular catabolism of glutathione (GSH), as it catalyzes the transfer of the gamma-glutamyl moiety from conjugated GSH to acceptors such as amino acids and dipeptides. It also breaks down GSH into its constitutive amino acids and thus provides the rate-limiting amino acid cysteine *de novo* synthesis of GSH [51]. GGT induction in cells occur as a protective adaptation against oxidants that are produced during normal metabolism or if oxidative stress increases due to any factor like the presence of reactive oxygen species [52]. The levels of GGT in serum are determined by several factors such as inflammation, alcoholic liver disease, gallbladder and biliary tract diseases, plasma lipid/lipoproteins content, hypertension, hyperuricemia, diabetes and various medications [50,51]. Results of assay for γ-glutamyl transferase (GGT) activity in the intestinal tissue extract for different treatment groups of rats are shown in Fig 6.33. It was seen that there was

significant difference ($p \leq 0.05$) in the content of GGT among all the groups. The control group recorded the highest content (13.32 nmole/unit/mL). The content in both the SAPE treated group (5.21 nmole/unit/mL) and indomethacin treated group (6.39 nmole/unit/mL) was higher than the colitis induced group without any treatment (2.16 nmole/unit/mL). Thus SAPE may be involved in meditating the synthesis and activity of GGT in diseased condition.

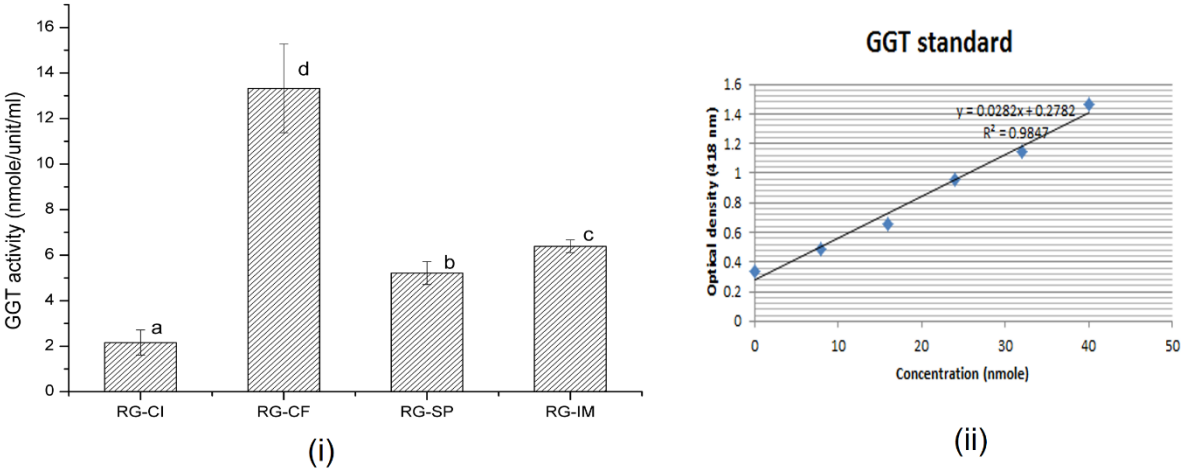

Fig 6.33 Results for assay of γ-glutamyl transferase (GGT) activity in the intestinal tissue extract for different treatment groups of rats (RG-CI: colitis induced group without any treatment; RG-CF: colitis free control group without any treatment; RG-SP: colitis induced group treated with SAPE; Group RG-IM: colitis induced group treated with indometacin)

The glutathione S-transferases (GSTs) are major phase II detoxification enzymes mostly found in the cytosol. They catalyses the conjugation of electrophilic substrates to glutathione (GSH), and also have other functions like peroxidase and isomerase activities, protecting cells against H_2O_2-induced cell death by inhibition of the Jun N-terminal kinase, and non-catalytically binding of endogenous and exogenous ligands. They result in the formation of GSH conjugates and the reduction of hydroperoxides by catalysing nucleophilic aromatic substitutions, epoxide ring-opening reactions and Michael additions to α, β - unsaturated ketones. The glutathione conjugates are eliminated by several transport mechanisms such as ATP-dependent GS-X pump, multispecific organic anion transporter, anion transporter of dinitrophenol S-GSH conjugates, P-glycoprotein (multidrug resistance pump) and MRP (multidrug-resistance-associated protein) [53,54]. Results of assay for glutathione S-transferase (GST) activity in the intestinal tissue extract for different treatment groups of rats are shown in Fig 6.34. Significant difference ($p \leq 0.05$) in the GST activity was observed among all the groups. The control group recorded the highest activity (0.29 µmole/mL/min), while the colitis induced group without any treatment evinced the lowest activity (0.17 µmole/mL/min).

The activity was higher in the SAPE treated group (0.26 µmole/mL/min) than the indomethacin treated group (0.24 µmole/mL/min). Thus, SAPE may also be responsible for alleviating the activity of GST enzyme for carrying out antioxidative activity.

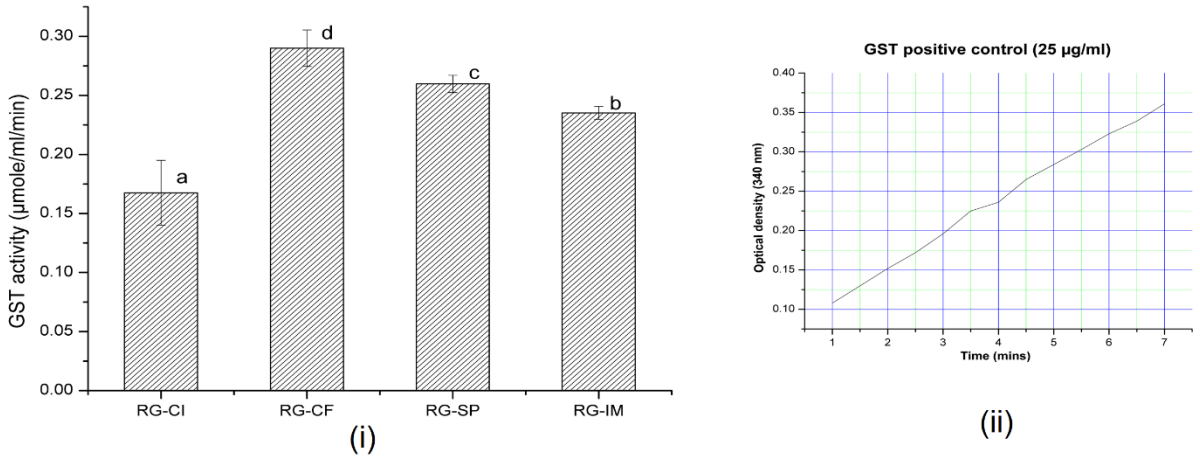

Fig 6.34 Results for assay of glutathione S-transferase (GST) activity in the intestinal tissue extract for different treatment groups of rats (RG-CI: colitis induced group without any treatment; RG-CF: colitis free control group without any treatment; RG-SP: colitis induced group treated with SAPE; Group RG-IM: colitis induced group treated with indometacin)

6.3.5.4.2 Anti-inflammatory effects

Interleukin-6 (IL-6) is a pleiotropic cytokine produced at the site of inflammation and plays a key role in the acute phase response, regulation of immune responses and hematopoiesis [55]. It is also involved in the regulation of metabolic, regenerative, and neural processes. Acute phase changes reflect the presence and intensity of inflammation and IL-6 is the chief stimulator of the production of most acute phase proteins [44]. IL-6 may be produced by a variety of cells following stimulation such as infection, trauma, or immunological challenge. It also has been found to have a protective role in the LPS-galactosamine septic shock model in mice [55]. IL-6 stimulates target cells via a membrane bound interleukin-6 receptor called as gp80. This receptor is expressed on monocytes, B cells, hepatocytes, neutrophils and certain subset of T cells. Upon binding, gp130 dimerizes, leading to the activation of the ras/raf/Mitogen-activated protein (MAP) kinase (MAPK) pathway. Most T cells, endothelial cells and fibroblasts do not express the IL-6R and respond to IL-6 through a process known as trans signalling which involves generation of soluble form of the IL-6 receptor [45,56]. Results of assay for interleukin 6 (IL-6) content in the intestinal tissue extract for different treatment groups of rats are shown in Fig 6.35. Its content was lowest in the control group (26.91 pg/mL).

There was no significant difference in content between the SAPE treated (90.76 pg/mL) and indometacin treated (82.83 pg/mL) groups, both of which evinced much lower content than the colitis induced group without any treatment (109.56 pg/mL).

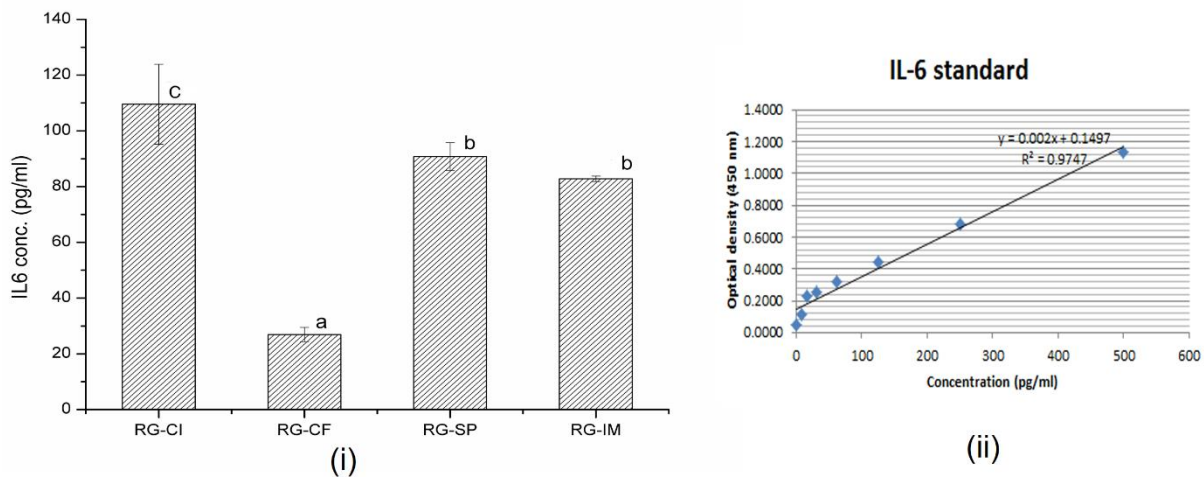

Fig 6.35 Results for assay of interleukin 6 (IL-6) content in the intestinal tissue extract for different treatment groups of rats (RG-CI: colitis induced group without any treatment; RG-CF: colitis free control group without any treatment; RG-SP: colitis induced group treated with SAPE; Group RG-IM: colitis induced group treated with indometacin)

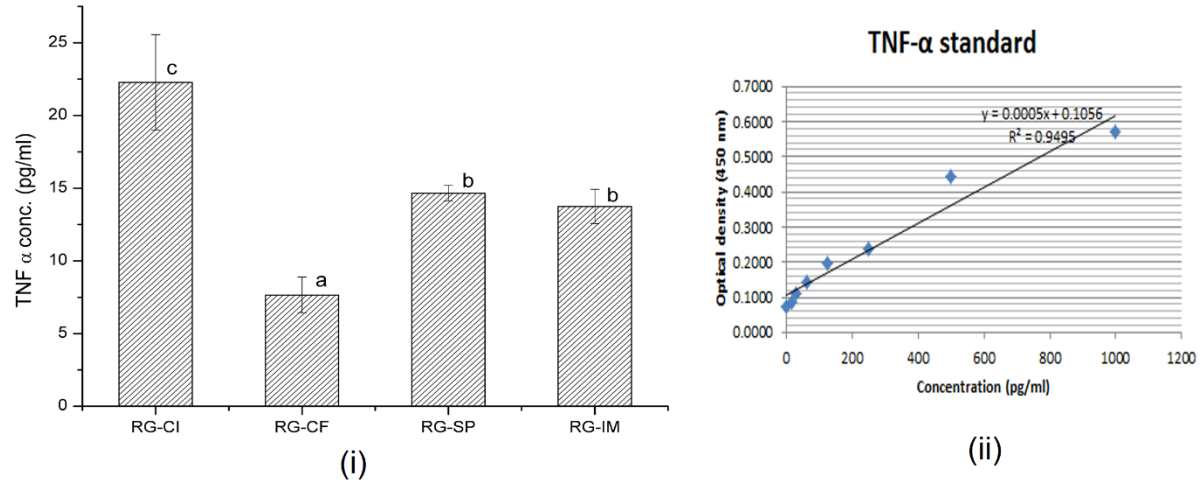

Fig 6.36 Results for assay of tumor necrosis factor alpha (TNF-α) content in the intestinal tissue extract for different treatment groups of rats (RG-CI: colitis induced group without any treatment; RG-CF: colitis free control group without any treatment; RG-SP: colitis induced group treated with SAPE; Group RG-IM: colitis induced group treated with indometacin)

Tumor necrosis factor alpha (TNF-α) is a proinflammatory cytokine involved in the innate immune response [57]. Macrophages are the major producers of TNFα and on a cellular level they regulate a number of critical cell functions including cell survival, cell proliferation, differentiation, and apoptosis, which are mediated by the two transmembrane receptors, TNF-R1 and TNF-R2. In general, TNFα does not generally provoke cell killing, but promotes gene

transcription and cell activation [58,59]. Under diseased condition, TNFα production and TNF receptor signaling regulates many facets of macrophage function. It plays a pivotal role in orchestrating the production of a proinflammatory cytokine cascade in many inflammatory diseases like Crohn's disease, rheumatoid arthritis, atherosclerosis, sepsis, psoriasis, diabetes, and obesity. It is one of the most abundant early mediators in inflamed tissue as it is rapidly released after trauma, infection, or exposure to bacterial-derived LPS [59]. Results of assay for tumor necrosis factor alpha (TNF-α) content in the intestinal tissue extract for different treatment groups of rats are shown in Fig 6.36. The TNF-α content was lowest in the control group (7.65 pg/mL). The content of TNF-α in both the SAPE treated (14.66 pg/mL) and indometacin treated (13.75 pg/mL) groups, was lower than the colitis induced group without any treatment (22.28 pg/mL). The results of both the IL6 and TNF- α assays clearly indicated a decrease in the level of inflammation after treatment with SAPE.

6. 4 Conclusions

$Zn(OTf)_2$-catalyzed selective esterification was found to be suitable for the production of salicylic acid phenylethyl ester (SAPE). This same procedure may thus be applied for the production of this novel ester on an industrial scale. In the *in silico* study, SAPE was predicted to have negligible toxicity and good levels of absorption, distribution after metabolism, bioavailability and low probability of effects on health. The molecular docking study revealed that SAPE could be docked at the active site of the COX-2 protein with scores comparable to or higher than the commercially available NSAIDs ibuprofen and indometacin. The stability of the enzyme ligand complex was evidenced by the molecular dynamics simulation study. Thus, SAPE can be considered as a novel compound with high potential to be used as NSAID against various inflammations. The newly synthesized SAPE molecule was tested by *in vitro* and *in vivo* assays for its bioactive role. The membrane stability assay exhibited the compound's stability towards human erythrocytes; while the MTT and Alamar Blue® assays showed that the compound was nontoxic towards the HepG-2 and CaCo-2 animal cell lines. The study with Wistar rats showed that pre administration SAPE is a good candidate for the prevention of colitis induced with bacterial LPS. Reduction in the extent of lipid peroxidation, increase in antioxidative activity and decrease in the level of pro-inflammatory cytokines was observed with the administration of SAPE, and these results were with par with the established NSAID indometacin. These results will further assist to establish SAPE as an easily synthesized novel NSAID.

References

1. Randjelović, P., Veljković, S., Stojiljković, N., Sokolović, D., Ilić, I., Laketić, D., Randjelović, D., and Randjelović, N. The beneficial biological properties of salicylic acid. *Acta Facultatis Medicae Naissensis*, 32(4): 259-265. 2015.
2. Paterson, J.R., and Lawrence, J.R. Salicylic acid: a link between aspirin, diet and the prevention of colorectal cancer. *QJM: An International Journal of Medicine*, 94(8): 445-448, 2001.
3. Abdu-Allah, H.H., El-Shorbagi, A.N., Abdel-Moty, S.G., El-Awady, R., and Abdel-Alim, A.A. 5-Aminosalyclic Acid (5-ASA): A unique anti-inflammatory salicylate. *Medicinal Chemistry (Los Angeles)*, 6: 306-315, 2016.
4. Zhang, T., Sun, L., Liu, R., Zhang, D., Lan, X., Huang, C., Xin, W., Wang, C., Zhang, D., and Du, G. A novel naturally occurring salicylic acid analogue acts as an anti-inflammatory agent by inhibiting nuclear factor-kappaB activity in RAW264. 7 macrophages. *Molecular Pharmaceutics*, 9(3): 671-677, 2012.
5. Rainsford, K.D., and Whitehouse, M.W. Anti-inflammatory/anti-pyretic salicylic acid esters with low gastric ulcerogenic activity. *Agents and Actions*, 10(5): 451-456, 1980.
6. Eshkol, N., Sendovski, M., Bahalul, M., Katz-Ezov, T., Kashi, Y., and Fishman, A., Production of 2-phenylethanol from L-phenylalanine by a stress tolerant *Saccharomyces cerevisiae* strain. *Journal of Applied Microbiology*, 106(2): 534-542, 2009.
7. Nursten, H.E. Volatile components in food. *Flavour and Fragrance Journal*, 1(4-5): 187, 1986.
8. Stofberg, J., and Grundschober, F. Consumption ratio and food predominance of flavoring materials: Second cumulative series. *Perfumer and Flavorist (USA)*, 12: 27–68, 1984.
9. Hall, R.L. Recent progress in the consideration of flavoring ingredients under the food additives amendment. *Food Technology*, 14(10): 488-495, 1960.
10. Opdyke, D.L. Monographs on fragrance raw materials. *Food and Cosmetics Toxicology*, 13(4): 449-457, 1975.
11. Ghosh, S., Kebaara, B.W., Atkin, A.L., and Nickerson, K.W. Regulation of aromatic alcohol production in *Candida albicans*. *Applied Environmental Microbiology*, 74(23): 7211-7218, 2008.

12. Fukuda, K., Watanabe, M., and Asano, K. Altered regulation of aromatic amino acid biosynthesis in β-phenylethyl-alcohol-overproducing mutants of sake yeast *Saccharomyces cerevisiae*. *Agricultural and Biological Chemistry*, 54(12): 3151-3156, 1990.
13. Rosenkranz, H.S., Carr, H.S., and Rose, H.M. Phenethyl alcohol I. effect on macromolecular synthesis of *Escherichia coli*. *Journal of Bacteriology*, 89(5): 1354-1369, 1965.
14. Silver, S. and Wendt, L. Mechanism of action of phenethyl alcohol: breakdown of the cellular permeability barrier. *Journal of Bacteriology*, 93(2): 560-566, 1967.
15. Silva, M.T., Sousa, J.C., Macedo, M.A., Polonia, J., and Parente, A.M. Effects of phenethyl alcohol on Bacillus and Streptococcus. *Journal of Bacteriology*, 127(3): 1359-1369, 1976.
16. Theodosis-Nobelos, P., Kourti, M., Tziona, P., Kourounakis, P.N., and Rekka, E.A. Esters of some non-steroidal anti-inflammatory drugs with cinnamyl alcohol are potent lipoxygenase inhibitors with enhanced anti-inflammatory activity. *Bioorganic and Medicinal Chemistry Letters*, 25(22): 5028-5031. 2015.
17. Tozkoparan, B., Aytaç, S.P., Gürsoy, Ş., and Aktay, G. Design and synthesis of some thiazolotriazolyl esters as anti-inflammatory and analgesic agents. *Medicinal Chemistry Research*, 21(2): 192-201. 2012.
18. Bundgaard, H., and Nielsen, N.M. Glycolamide esters as a novel biolabile prodrug type for non-steroidal anti-inflammatory carboxylic acid drugs. *International Journal of Pharmaceutics*, 43(1): 101-110, 1988.
19. Murtaza, G., Karim, S., Akram, M.R., Khan, S.A., Azhar, S., Mumtaz, A., and Bin Asad, M.H.H. Caffeic acid phenethyl ester and therapeutic potentials. *BioMed Research International*, 2014: 1-9, 2014.
20. Mamidi, N., and Manna, D. Zn (OTf) 2-promoted chemoselective esterification of hydroxyl group bearing carboxylic acids. *Journal of Organic Chemistry*, 78(6): 2386-2396, 2013.
21. Allinger, N.L. Conformational analysis. 130. MM2. A hydrocarbon force field utilizing V1 and V2 torsional terms. *Journal of the American Chemical Society*, 99(25): 8127-8134, 1977.
22. de la Nuez, A. and Rodríguez R. Current methodology for the assessment of ADME-Tox properties on drug candidate molecules. *Biotecnología Aplicada*, 25: 97-110, 2008.

23. Kharkar, P.S. *In silico* absorption, distribution, metabolism and excretion, in Lill, M.A., editor. *In silico Drug Discovery and Design*, pages 148-162, Future Science Group, London, UK, 2013.
24. Singh, S.P., Deb, C.R, Kakati, L.N., and Konwar, B.K. QSAR-based drug designing studies on HIV-1 integrase inhibitors. *Network Modeling Analysis in Health Informatics and Bioinformatics*, 5(1): 33, 2016.
25. Thomsen, R., and Christensen, M.H. MolDock: a new technique for high-accuracy molecular docking. *Journal of Medicinal Chemistry*, 49(11): 3315-3321, 2006.
26. SchuÈttelkopf, A.W., and Van Aalten, D.M. PRODRG: a tool for high-throughput crystallography of protein–ligand complexes. *Acta Crystallographica Section D: Biological Crystallography*, 60(8): 1355-1363, 2004.
27. Borah, R., Kumar, A., Das, M.K., and Ramteke, A. Surface functionalization-induced enhancement in surface properties and biocompatibility of polyaniline nanofibers. *RSC Advances*, 5(60): 48971-48982, 2015.
28. de S Vargas, F., DO de Almeida, P., Aranha, E.S.P., de A Boleti, A.P., Newton, P., de Vasconcellos, M.C., Junior, V.F.V., and Lima, E.S. biological activities and cytotoxicity of diterpenes from *Copaifera* spp. Oleoresins. *Molecules*, 20(4): 6194-6210, 2015.
29. Denizot, F., and Lang, R., Rapid colorimetric assay for cell growth and survival: modifications to the tetrazolium dye procedure giving improved sensitivity and reliability. *Journal of Immunological Methods*, 89(2): 271-277, 1986.
30. O'Brien, J., Wilson, I., Orton, T., and Pognan, F. Investigation of the alamar blue (resazurin) fluorescent dye for the assessment of mammalian cell cytotoxicity. *European Journal of Biochemistry*, 267: 5421–5426, 2000.
31. Upadhyay, A., Chattopadhyay, P., Goyary, D., Mazumder, P.M., and Veer, V. Anti-inflammatory effect of *Euphorbia hirta* leaf extract in rats and modulation of inflammation-associated prostaglandins (PGE-2) and nitric oxide (NO) expression in RAW264.7 macrophage. *Journal of Pharmaceutical Sciences and Pharmacology*, 1(1): 68-73, 2014.
32. Sun, Y., Lin, L.J., Lin, Y., Sang, L.X., Jiang, M., and Zheng, C.Q. *Gingko biloba* extract (Ginaton) ameliorates dextran sulfate sodium (DSS)-induced acute experimental colitis in mice via reducing IL-6/STAT3 and IL-23/IL-17. *International Journal of Clinical and Experimental Medicine*, 8(10): 17235-17247, 2015.

33. Gehlhaar, D.K., Verkhiver, G., Rejto, P.A., Fogel, D.B., Fogel, L.J., and Freer, S.T. Docking conformationally flexible small molecules into a protein binding site through evolutionary programming, in McDonnell, J.R., Reynolds, R.G. and Fogel, D.B., editorss. *Proceedings of the fourth International Conference on Evolutionary Programming*, pages 615-627, The MIT press, Cambridge, Massachusetts, London, England, 1995.
34. Yang, J.M., and Chen, C.C. GEMDOCK: a generic evolutionary method for molecular docking. *Proteins: Structure, Function, and Bioinformatics*, 55(2): 288-304, 2004.
35. Lee, J.W., Serna, F., Nickels, J., and Schmidt, C.E. Carboxylic acid-functionalized conductive polypyrrole as a bioactive platform for cell adhesion. *Biomacromolecules*, *7*(6): 1692-1695, 2006.
36. Qiu, G.H., Xie, X., Xu, F., Shi, X., Wang, Y., and Deng, L. Distinctive pharmacological differences between liver cancer cell lines HepG2 and Hep3B. *Cytotechnology*, 67(1): 1-12, 2015.
37. Sambuy, Y., De Angelis, I., Ranaldi, G., Scarino, M.L., Stammati, A., and Zucco, F. The Caco-2 cell line as a model of the intestinal barrier: influence of cell and culture-related factors on Caco-2 cell functional characteristics. *Cell Biology and Toxicology*, 21(1): 1-26, 2005.
38. Lea, T. Caco-2 Cell Line, in Verhoeckx, K., Cotter, P., López-Expósito, I., Kleiveland, C.,Lea, T., Mackie, A., Requena, T., Swiatecka, D., Wichers, H. editors. *The Impact of Food Bioactives on Health*, pages 103-111, Springer International Publishing, USA, 2015.
39. Al-Nasiry, S., Geusens, N., Hanssens, M., Luyten, C., and Pijnenborg, R. The use of Alamar Blue assay for quantitative analysis of viability, migration and invasion of choriocarcinoma cells. *Human Reproduction*, 22(5): 1304-1309, 2007.
40. Voytik-Harbin, S.L., Brightman, A.O., Waisner, B., Lamar, C.H., and Badylak, S.F. Application and evaluation of the alamar Blue assay for cell growth and survival of fibroblasts. *In Vitro Cellular & Developmental Biology-Animal*, 34(3): 239-246, 1998.
41. Kunanusorn, P., Teekachunhatean, S., Sangdee, C., and Panthong, A., Antinociceptive and anti-inflammatory activities of a Chinese herbal recipe (DJW) in animal models. *International Journal of Applied Research in Natural Products*, *2*(1): 1-8, 2009.
42. Morley, J.E., Thomas, D.R., and Wilson, M.M.G. Cachexia: pathophysiology and clinical relevance. *The American Journal of Clinical Nutrition*, 83(4): 735-743, 2006.

43. Peyrin-Biroulet, L., Panés, J., Sandborn, W.J., Vermeire, S., Danese, S., Feagan, B.G., Colombel, J.F., Hanauer, S.B., and Rycroft, B., Defining disease severity in inflammatory bowel diseases: current and future directions. *Clinical Gastroenterology and Hepatology*, 14(3): 348-354, 2016.
44. Gabay, C., Interleukin-6 and chronic inflammation. *Arthritis Research and Therapy*, *8*(2): 1, 2006.
45. Scheller, J., Chalaris, A., Schmidt-Arras, D., and Rose-John, S. The pro-and anti-inflammatory properties of the cytokine interleukin-6. *Biochimica et Biophysica Acta (BBA)-Molecular Cell Research*, 1813(5): 878-888, 2011.
46. Mani, R., Meena, B., Valivittan, K., and Suresh, A. Glutathione-S-Transferase and catalase activity in different tissues of marine catfish (*Arius arius*) on exposure to cadmium. *International Journal of Pharmacy and Pharmaceutical Sciences*, 6(1): 326-332, 2014.
47. Grotto, D., Maria, L.S., Valentini, J., Paniz, C., Schmitt, G., Garcia, S.C., Pomblum, V.J., Rocha, J.B.T., and Farina, M., Importance of the lipid peroxidation biomarkers and methodological aspects for malondialdehyde quantification. *Quimica Nova*, 32(1): 169-174, 2009.
48. Ayala, A., Muñoz, M.F., and Argüelles, S. Lipid peroxidation: production, metabolism, and signaling mechanisms of malondialdehyde and 4-hydroxy-2-nonenal. *Oxidative Medicine and Cellular Longevity*, 2014: 1-31, 2014.
49. Kakkar, R., Kalra, J., Mantha, S.V., and Prasad, K. Lipid peroxidation and activity of antioxidant enzymes in diabetic rats. *Molecular and Cellular Biochemistry*, 151(2): 113-119, 1995.
50. Grundy, S.M. Gamma-glutamyl transferase another biomarker for metabolic syndrome and cardiovascular risk. *Arteriosclerosis, Thrombosis, and Vascular Biology*, 27(1): 4-7. 2007.
51. Jiang, S., Jiang, D., and Tao, Y. Role of gamma-glutamyltransferase in cardiovascular diseases. *Experimental and Clinical Cardiology*, 18(1): 53, 2013.
52. Whitfield, J.B. Gamma glutamyl transferase. *Critical Reviews in Clinical Laboratory Sciences*, 38(4): 263-355, 2001.
53. Sheehan, D., Meade, G., and Foley, V.M. Structure, function and evolution of glutathione transferases: implications for classification of non-mammalian members of an ancient enzyme superfamily. *Biochemical Journal*, 360(1): 1-16, 2001.

54. Sherratt, P.J., and Hayes, J.D. Glutathione S-transferases, in Ioannides, C. editor. *Enzyme Systems that Metabolise Drugs and Other Xenobiotics*, pages 319-352, John Wiley & Sons, Chichester, England, 2001.
55. Tilg, H., Trehu, E., Atkins, M.B., Dinarello, C.A., and Mier, J.W. Interleukin-6 (IL-6) as an anti-inflammatory cytokine: induction of circulating IL-1 receptor antagonist and soluble tumor necrosis factor receptor p55. *Blood*, 83(1): 113-118, 1994.
56. Barnes, T.C., Anderson, M.E., and Moots, R.J. The many faces of interleukin-6: the role of IL-6 in inflammation, vasculopathy, and fibrosis in systemic sclerosis. *International Journal of Rheumatology*, 2011: 1-6, 2011.
57. Olmos, G., and Lladó, J. Tumor necrosis factor alpha: a link between neuroinflammation and excitotoxicity. *Mediators of Inflammation*, 2014:1-12, 2014.
58. Wu, H., and Hymowitz, S.G. Structure and Function of Tumor Necrosis Factor (TNF) at the Cell Surface, in Bradshaw, R.A., and Dennis, E.A., editors. *Handbook of Cell Signaling 2nd edition*, pages 265-275, Academic Press, Oxford, 2009.
59. Parameswaran, N., and Patial, S., Tumor necrosis factor-α signaling in macrophages. *Critical Reviews in Eukaryotic Gene Expression*, 20(2): 87-103, 2010.